Strain-rate controlled Gleeble experiments to determine the stress-strain behavior of HSLA steel S960QL

Sebastian Neubert, Andreas Pittner and Michael Rethmeier, Berlin, Germany

Article Information

Correspondence Address

Dr.-Ing. Andreas Pittner
Bundesanstalt für Materialforschung
und -prüfung (BAM)
Division 9.3 "Welding Technology"
Unter den Eichen 87
12205 Berlin, Germany
E-mail: Andreas.pittner@bam.de

Keywords

Gleeble testing; HSLA; strain-rate; stress-strain behavior; transformable steels; nu-merical welding simulation In order to generate a material data base for computational welding mechanics, temperature and strain-rate dependent stress-strain experiments were performed by using a Gleeble®3500 testing system. The object of the investigation was HSLA transformable steel S960QL and related solid phases as bainite, martensite and austenite. For the production of these solid phases, the base material was heat treated according to an average weld temperature cycle which was extracted within the heat affected zone of a thermal numerical weld simulation of a GMA weld. The hot tensile tests were carried out via cost-saving flat specimen geometries. Two experimental series with different strain-rates were conducted, where the longitudinal strain-rate was controlled by specification of the transversal strain-rate applying Poisson's-ratio. Subsequently, the resulting stress-strain curves were approximated in accordance with the Ramberg-Osgood-materials law. Consequently, it is shown that the temperature and strain-rate dependent stress-strain behavior of metals can be successfully characterized by means of a Gleeble®-system. However, this requires a control of the longitudinal strain-rate by specification of the transversal strain-rate. The related experimental procedure and the method of evaluation are explained in detail. With regard to all tested solid phases, a significant strain-rate dependency can only be observed upwards from temperatures of 400 °C. Based on experimental results, Ramberg-Osgood-parameters will be presented to describe the stress-strain behavior of steel S960QL and related solid phases for temperatures between 25 °C and 1200 °C. Furthermore, the use of costsaving flat specimen-geometry appears reasonable.

Owing to the need to reduce CO_2 emissions by minimizing overall energy and resource consumption, and simultaneously motivated by a desire to improve the stability and the lifespan of steel compounds, a growing demand for strength enhanced steels is observable. With respect to material design, the use of transformable high-strength low-alloy (HSLA) steel is advantageous, because it still

enables the best compromise between light-weight constructions and processability. Exploiting bearing capacity and by dint of a high degree of mechanization as well as a satisfactory controllability of heat input, fusion processes through conventional GMA-welding are often used. Unfortunately, the heat input of the welding process causes undesirable welding distortion and detri-

mental welding residual stress. Analyzing these phenomena during production run-up can be done by numerical welding simulation, which requires the implementation of temperature dependent on material properties. The availability of these material data is a 'bottleneck' with respect to the efficient application of digital twins in the real welding process [1].

The availability of thermodynamic quantities seems to be a minor issue because calorimetric experiments are relatively inexpensive and easy to conduct. Additionally, these quantities are mainly affected by the chemical composition of the material in question. Knowing the composition enables the possibility of a sufficient approximation of the thermodynamic properties thanks to calculation programs [2] and existing material databases. In addition to composition, thermometallurgical/-mechanical properties are also dependent on the production process, subsequent processing and mechanical load [3-5]. In this case, material properties can be approximated by calculation programs, constitutive descriptions [5] and existing databases from similar materials. Under batch variations, especially in the case of newly developed materials, large uncertainties arise and the influence on a calculated mechanical response is hardly assessable. Regarding this, authors in [1, 6-8], emphasize the strong impact of thermometallurgical /-mechanical properties on calculated welding residual stress and distortion, which is confirmed by exemplary examinations as seen in [8-12]. To exclude approximation induced uncertainties in calculated results, material properties should be experimentally determined for each case. However, the application of partly complex specimen geometries, the conducting of a multitude of different experiments and the use of several facilities are obstacles to carrying out experiments because they demand high requirements in time and money.

In order to provide a material database for GMA welding simulation, the experimental characterization of the stress-strain behavior of fine-grained HSLA steel S960QL with related solid phases is focused on in this study. Authors in [12-15] have proven that welding induced microstructural changes have a strong influence on the stress-strain behavior of material within the heat affected zone (HAZ). Furthermore, the material within the HAZ is subjected to averaged heating rates of up to 1000 K/s for GMA-welding processes. Because of the strong correlation between strain- and temperature-rate, during heating the HAZ-material experiences thermally induced strain-rates of up to 1.5 %/s [12]. In this context, experimenters in [7, 12, 16] revealed a significant influence of strain-rate on the stress-strain behavior of high-strength steel at temperatures above 400 °C. The influence of visco-plasticity at high temperature ranges on calculated welding residual stress and weld distortion was investigated by [17]. The author concluded that visco-plasticity can be neglected by calculation of welding residual stress but should be considered in case of welding distortion. Thus, experiments should be strain-rate controlled and the steel to be tested should be thermally and mechanically loaded with respect to the HAZ conditions of GMA weldments.

Inspired by the works of Nippes and Savage [18, 19] the Gleeble®-system was developed at Rensselaer Polytechnic Institute (RPI) to simulate conditions of an HAZ including mechanical loading. Basing on the first commercial Gleeble® testing system produced in 1957, the Gleeble® technique has evolved, enabling experiments concerning microstructural simulation of HAZ's, hot ductility properties, TTT and CCT diagrams, thermal fatigue and many other thermometallurgical/mechanical studies. Using a Gleeble® testing system, the specimen to be tested is clamped between two water cooled jaws and heated by conductive resistance heating. Because of this principle, the temperature distribution in the axial direction of the specimen is non-uniform where the peak temperature is located at the center of the specimen. It should be pointed out that this non-uniform temperature distribution is a large barrier for performing strain-rate controlled stress-strain experiments at elevated temperatures. Intended strain-rate controlling by the use of a predefined axial misalignment per time unit or by the use of a predefined increase of load per time unit will inevitably lead to variable strain-rates at the local position of the peak temperature where the material behavior has to be evaluated. A literature review of the last decades shows that many hot ductile tests using the Gleeble®-test system were carried out yielding supposedly constant strain-rates. Nevertheless, experimenters have avoided the method to the present for strain-rate control. However, attempts have been made to diminish the axial temperature gradient by developing more suitable specimen geometries [20, 21]. In addition to increased geometric complexity compared with typical 'dog-bone'-shapes, the newly developed specimen geometry has failed in self-conducted experiments when applying GMAheating rates because the shunt strips of the specimen have been melted. So far, it seems that experimenters have had to live with a pronounced axial non-uniform temperature distribution by performing experiments at elevated temperatures.

Thermal and mechanical introduced strains can be measured by contactless optical extensometers as well as tactile measuring equipment which usually yield a better spatial resolution than the optical ones. As for tactile methods, longitudinal strains are often measured by the use of L-gauges in combination with ceramic disks attached to the specimen. In the case of inhomogeneous axial temperature distribution in the specimen, the transversal strain at peak temperature is measured by C-gauges.

In the present investigation, in order to create a material database for numerical weld simulation, the thermophysical simulator Gleeble®3500 will be used to carry out strain-rate controlled stress-strain experiments of HSLA steel S960QL and related solid phases as martensite, bainite and austenite. For the production of these solid phases the base material is heat treated by characteristics of an average weld temperature cycle which is extracted within the HAZ of a thermal numerical weld simulation of a GMA weld. The longitudinal strain-rate is controlled by specification of the transversal strain-rate by using Poisson's-ratio. Because of the non-uniform temperature distribution along the axial direction of the specimen, the record and control of the transversal strain has been made with a tactile C-gauge. Paying attention to the strain-rate conditions within the HAZ and experimentally revealing the strain-rate dependency of the tested materials, leads to two experimental series which differ in temperature independent and temperature dependent strain-rate concepts. Experiments were conducted using cost-saving simple flat specimen geometry ('dog-bone'-shape) which was already successfully used to characterize the transformation induced plasticity of the same batch of examined steel S960QL [22].

Experimental procedure

This section on experimental procedures consists of a description of the GMA-welding experiments and of the design of the Gleeble®-experiments. In order to generate a material data base for the numerical weld simulation, the global temperature field extracted in the GMA-welding experiments will be used to design the thermal cycles needed for the Gleeble®-experiments. For the latter, the material to be tested will be heat treated incorporating characteristics of weld temperature cycles in order to produce solid phases like bainite, martensite and austenite. Additionally, the GMA tem-

С	P	S	N	В	Cu	Nb	Ti	V	Al	Si	Mn	Cr	Mo	Ni
	Base material (S960QL)													
0.14	0.009	0.001	0.01	0.0001	0.03	0.013	0.002	0.046	0.03	0.3	0.87	0.49	0.53	0.52
	Weld metal													
0.13	0.012	0.007	0.0044	0.0001	0.08	0.007	0.038	0.021	0.013	0.57	1.35	0.43	0.55	1.51

Table 1: Measured chemical elements in wt %

perature field will be analyzed regarding the magnitude of strain-rates occurring within the heat affected zone (HAZ) of the weld joint. Finally, to carry out strain-rate controlled stress-strain experiments with the Gleeble®-test system, the strain-rate controlled method used in the experiments will be explained in detail.

Welding. The materials selected were fine grained low-alloyed high-strength steel S960QL as base material according to DIN EN 10025-6, and a matching filler metal which is classified according to the standard DIN EN ISO 16834 (A G Mn4Ni2CrMo). Corresponding chemical elements, evaluated by in-house spark spectroscopy conducted on both the base material and the weld metal are presented in Table 1. Qualifying the toughness properties of the base material S960QL at a temperature of -40 °C, four notched-bar impact tests (Charpy V-notch specimen) according DIN EN ISO 148 were carried out. With a minimal notched bar impact work of 71 J, the requirements of DIN EN ISO 10025-6 were fulfilled.

The single-pass butt weld joints were executed using a matching filler wire and a V-groove preparation with an opening angle of 30°. The reference data used for validation was generated by considering the mean values of GMA-experiments. The pulsed GMA welding was prepared using a wire feed rate of 9 m/min. The travelling speed of 0.55 m/min and the average values of 254.6 A electrical current and 27 V electrical voltage yield an energy input per unit length of 0.75 kJ/mm. To ensure a constant weld seam quality, the plates were

tack welded at the beginning, the middle and the end of the plate. The weld root formation was supported by a ceramic backing plate. The middle of one side of the tack welded sheets was clamped using a single clamping lever, where a small flat surface together with high clamping force secured the weld joint from slipping and tilting. This clamping technique can be approximated by a rotation-free "one point fixation". The dimensions and the quasi "one point fixation" of the weld joints are shown in the schematic illustration in Figure 1.

In order to record the transient temperature, field type K thermocouples having a diameter of 0.25 mm were tack welded along the dashed line (see Figure 1) on the top and bottom surface. The positions are given in Table 2. The sampling rate of the thermocouple signal was set to 50 Hz.

Design of Gleeble®-experiments. In the first part of this section, a thermal finite element model of a GMA-weld joint will be developed and subsequently utilized to evaluate the global temperature field of the heat affected zone (HAZ) with respect to the average temperature cycle and the average strain-rate. The second part comprises the definition of the experimental plan where solid phases, temperature ranges and strain-rates to be tested will be specified. Subsequently, geometries of specimens in the Gleeble®-experiments will be numerically verified with respect to the smallest possible passive cooling down time $t_{8,5}$ from T = 800 °C down to T = 500 °C, which results in optimized specimen geometry. Lastly, various meth-

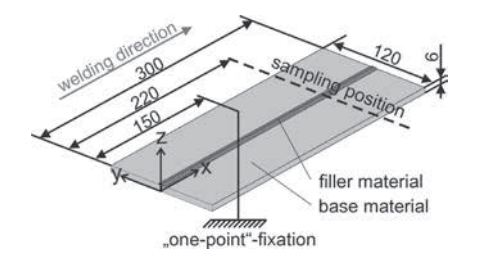


Figure 1: Schematic illustration of the weld joint. The "one-point-fixation" is shown by the trivalent bearing of the plate at x = 150. The sampling position of the quantities for validation is x = 220 (dashed line). Dimensions given in mm

ods of performing stress-strain experiments using a Gleeble®3500-test system will be presented. As a result, the appropriate method for a strain-rate controlled determination of the stress-strain behavior can be explained.

Modelling and evaluation of a thermal FE-model describing a GMA-weld joint

Numerical modelling of a GMA-weld joint. The numerical simulation was performed using a commercial FEA-code SYSWELD®. The simulation was based on a three-dimensional mesh geometry (see Figure 2) with matching dimensions of the GMAweld joints (see Figure 1). Within the range of the weld seam and heat affected zone (HAZ) an element edge length of 0.5 mm × 0.5 mm was chosen for the (y-z)plane. The area of the weld pool region is modelled separately, which requires an unstructured mesh in that region. In this area and within the HAZ, the element edge length in x-direction is 2 mm. To reduce computation time, the mesh in the outer regions was gradually coarsened. The full model consists of around 127,000 linear elements and 140,000 nodes.

The numerical calculation of the solidstate transformations was carried out by the use of transformation kinetic models. Here, a

Z		
	2	Omn

Figure 2: Meshed geometry used for FEA

z = 6	z = 0
a: 4.8 b: 6 c: 7 d: 8.3	e: 2 f: 3 g: 4.4

Table 2: Positions of thermocouples at the high end of the sampling position (see Figure 1) with top surface at z=6 and bottom surface at z=0. Letters (a-g) used as identifiers in Figure 5. Dimensions given in mm

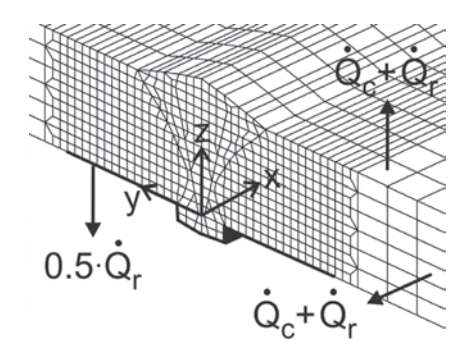


Figure 3: Section of meshed plate with schematic representation of ceramic backing plates (black) and thermal boundary conditions. Heat transfer of type convection \dot{Q}_r and radiation \dot{Q}_r

distinction between solid state transformation with and without diffusion is essential. The mathematical handling of the diffusion controlled austenitic ($\alpha \rightarrow \gamma$)-transformation was based on the semi-empiric transformation kinetic model according to Leblond-Devaux [23]. With the consequent evolutionequation, the transformation kinetics can be incorporated into the FEA-model by the use of information taken from isothermal and continuous transformation temperature diagrams. By analyzing Gleeble®-experiments based on the GMA-thermal cycles measured and by analyzing cross-sections of the GMAwelding joints, a pure austenitic-martensitic $(\alpha \rightarrow \gamma)$ -transformation was confirmed. In case of the martensitic ($\alpha \rightarrow \gamma$)-transformation (without diffusion), the Koistinen-Marburgermodel [24] was applied. Evaluating Gleeble®experiments on the base material revealed a martensite start temperature of 420 °C (see Figure 18) and a transformation constant of 0.02856. The associated martensite start temperature and the transformation constant were incorporated into the transformation kinetic model given by Koistinen-Marburger.

The welding process is approximated by a pure heat conduction problem. Following the approach of Karkhin [25], the apparent heat source which is defined by a volumetric energy distribution comprises phenomena like fluid flow in the weld pool, solidification as well as heat input due to the arc. In this study, a one volume distributed Gaussian heat source [25] and several double ellipsoidal heat sources [26] were applied. The constellation of the superimposed heat sources is explained in more detail in [10]. The heat sources move along the welding trajectory in x-direction as indicated in Figure 2. The top and bottom surfaces are imposed with heat transfer by \dot{Q}_c convection and \dot{Q}_r radiation . The region of the root at the bottom surface is subjected to significantly reduced radiation and no convection because of the nearly adiabatic effect of the ceramic backing plates. A schematic representation of boundary conditions is shown in Figure 3. The thermal simulations were conducted using thermal conductivity λ_{th} and specific heat capacity c_n (see Figure 4) taken from the SYSWELD® database for steel S355J2G3, which is published in [27]. This can be done because of the chemical similarity of the S355J2G3, S960QL steel and the filler wire ED-FK 1000® used. Within the SYSWELD®-environment, the latent heat effect is taken into account via the specific heat approach [28].

One validation criterion deals with the numerical reproduction of the global temperature field. In Figure 5, the experimental temperature signals are plotted for the temperature signals calculated, where the evaluation positions correspond to the positions of the tack-welded thermocouples (see Table 2). With a difference of peak

temperature at $\Delta T_{peak} \leq 4$ %, a very satisfactory qualitative and quantitative accord between measured and numerically calculated temperature signals can be stated. The sum of the heat of all apparent heat sources, superimposed in order to numerically determine the heat input of the arc, resulted in a numerical heat input of $Q_{num} \approx 185.9 \ kJ.$ The net heat input of the GMA welding process is $Q_{exp} \approx 225 \ kJ.$ Therefore, the ratio of Q_{num} and Q_{exp} results in 0.83, which appears to be feasible for a pulsed GMA-process.

In addition to the thermal cycles, the molten pool area too has to be numerically reproduced, where the molten pool shape is given as an isothermal surface corresponding to the solidification temperature of the present material with T = 1490 °C (see Figure 6). The black dotted curve in Figure 6 represents the average experimental molten pool shape indicated by several cross-sections along the weld seam (see left side Figure 6). The grey area (see right side Figure 6) represents the numerically simulated molten pool shape. The differences in surfaces are smaller than four percent, which lies within the experimental scattering band. Consequently, an excellent qualitative and quantitative agreement between a simulated and measured molten pool shape is visible.

Average temperature cycle. In order to generate a material database for the numerical welding simulation of a GMA weld joint made of S960QL steel, the temperature dependent stress-strain behavior of the related solid phases (bainite, martensite, austenite) must be measured. The main focus of attention when reproducing these solid phases is directed to thermally load the S960QL steel tested in accordance

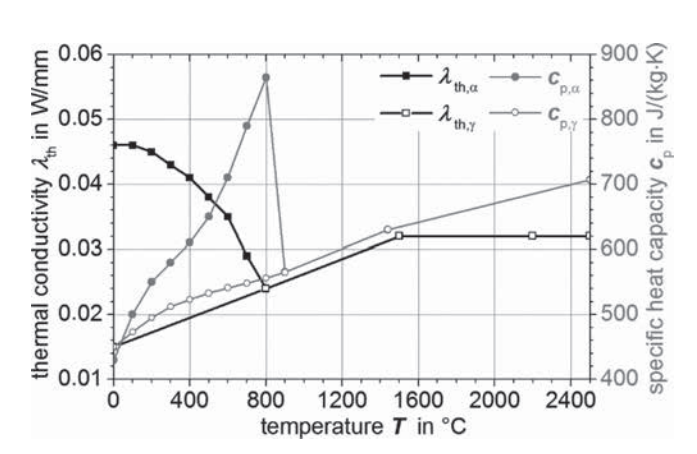


Figure 4: Thermal conductivity and specific heat capacity for α - and γ -phases according to [27]

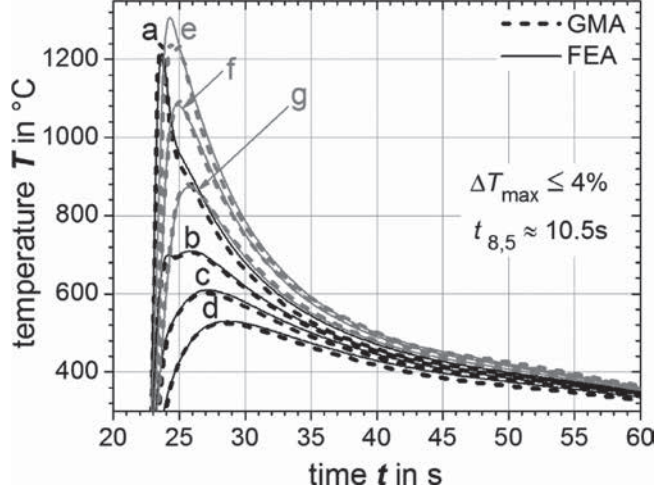


Figure 5: Measured (dashed lines) and simulated (full lines) thermal cycles. Letters (a-g) indicating positions of thermocouples (Table 2)

with an average thermal welding cycle which represents thermally HAZ conditions. Thus, the extent of austenitic grain growth and precipitation should be similar to the HAZ-position, where the average thermal welding cycle occurs. Hence, the transient thermal field of the GMA weld experiments performed was reconstructed, which allows us to locate and to evaluate the representative thermal history within the volume of the HAZ of the GMA welded plates (see black dots in Figure 6). To find the position of the average thermal cycle, a microsection of the real weld seam was analyzed with respect to the austenite grain size distribution at the middle of the HAZ-volume. Transverse to the welding direction, the position of the average austenite grain size was determined and consequently chosen as evaluation position. The resulting average thermal cycle extracted from the results given by numerical simulation is presented in Figure 7, where the characteristics are the heating rate T_{heating}

the holding time $t_{\rm H}$ above 1000 $^{\circ}\text{C}\text{,}$ the maximum peak temperature T_{peak} and temperature evolution above 800 °C. These characteristics must be replicated within the Gleeble®-experiments. The black curve in Figure 8 shows a thermal cycle reproduced by using the Gleeble®3500-test system. Here, a cooling down time of $t_{8.5}$ = 6 s was set to ensure the generation of a pure fraction of martensite through passive cooling. In order to decrease the Skin-effect, the heating rate below 800 °C was reduced to a third. Consequently, a more uniformly heated cross-section of the specimen could be obtained. Apart from that, all other aforementioned characteristics are well described.

Thermally induced strain-rates. Subsequently, the results of the numerical welding simulation of a GMA weld joint will be used to estimate xthe average strain-rates of the material within the HAZ. This will lead to strain-rates which have to be considered within the experimental plan to

measure the strain-rate and the temperature dependent stress-strain behavior of S960QL steel and related solid phases. The relation (see Equation 2) between temperature-rate \dot{T} and strain-rate $\dot{\epsilon}$ with the proportional factor α (coefficient of thermal expansion) can be derived by application of the total time derivation on the definition of the coefficient of thermal expansion (see Equation 1).

$$\alpha = \frac{\Delta L}{L \cdot \Delta T} \tag{1}$$

$$\alpha \cdot \Delta T = \frac{\Delta L}{L} = \varepsilon \left| \frac{d(...)}{dt} \right|$$
 (2)

with
$$\alpha = \alpha_{const} = 1.63 \times 10^{-5} \text{K}^{-1} \rightarrow \alpha_{const} \times \dot{T} \approx \epsilon$$

 α – coefficient of thermal expansion; L – length of a specimen; T – temperature; \dot{T} – temperature-rate; ϵ – strain; $\dot{\epsilon}$ – strain-rate

Applying Equation 2 to the thermal cycles extracted at positions A, B and C (see

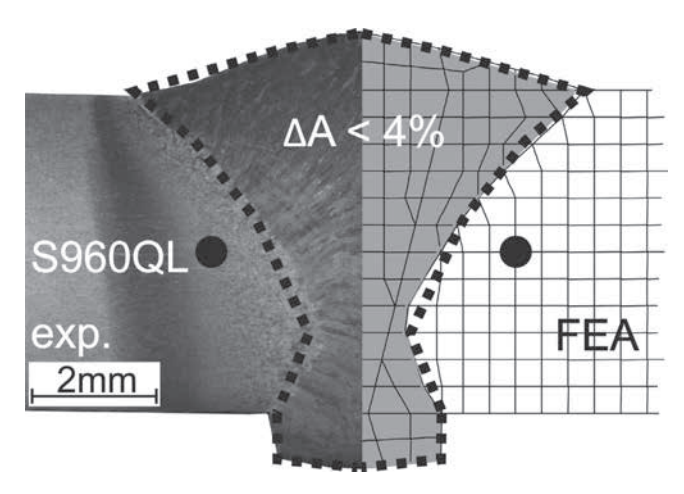


Figure 6: Average experimental (black dotted curve) and numerically calculated (grey area) molten pool shape, which corresponds with the isothermal surface of $T=1490\,^{\circ}\mathrm{C}$ (solidification temperature). Black points indicating position for extraction of average temperature cycle within HAZ (see Figure 7)

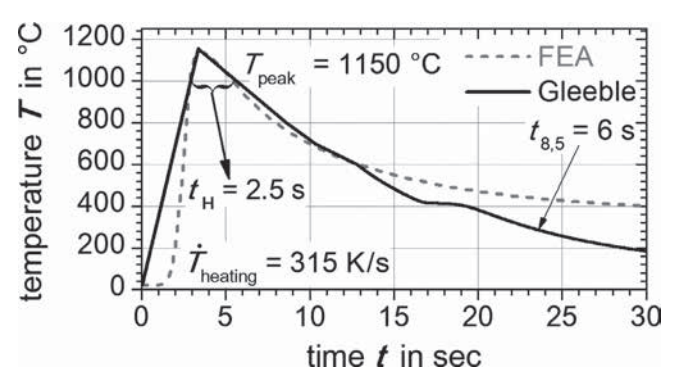


Figure 8: Average temperature-peak cycle (grey dashed curve) reproduced (black curve)using Gleeble®3500-system by use of specimen geometry "1" (see Figure 13)

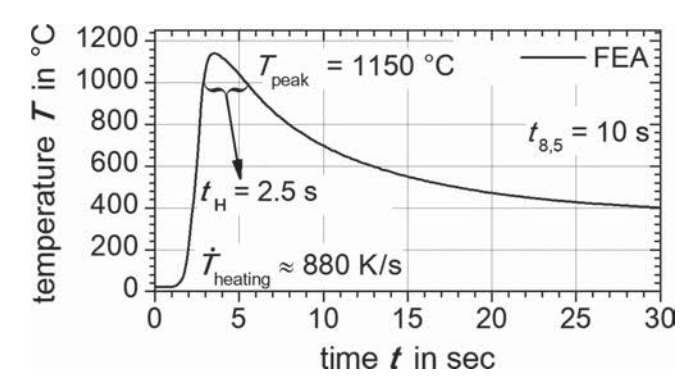


Figure 7: Average temperature cycle extracted from FEA. Characteristics are maximum peak temperature – T_{peak} , holding time above 1000 °C – t_{th} cooling time from 800 °C to 500 °C – $t_{g,5}$ and heating up rate – $\dot{T}_{heating}$

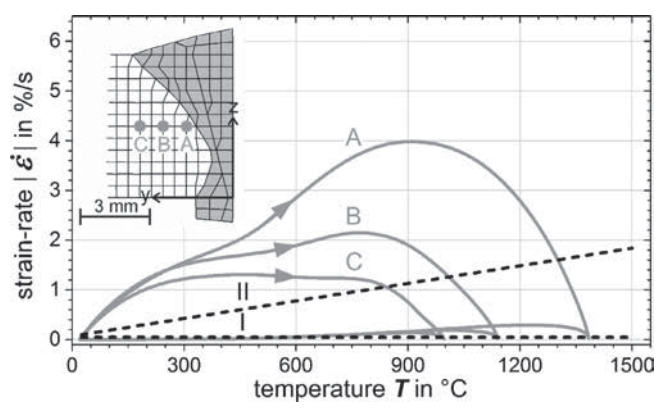


Figure 9: Approximated strain-rates (Equation 2) for positions A, B (average temperature cycle of HAZ) and C within the HAZ calculated at x = 220 mm (see Figure 1). Curve sections indicated by arrows describing heating-up range of thermal welding cycles. Dashed black lines describing approximated strain-rates $\dot{\epsilon}_l$ and $\dot{\epsilon}_{ll}$.

Figure 9) results in approximated strain-rates pertaining to positions A, B and C as evaluated. In Figure 9, the absolute value of the strain-rates $|\dot{\epsilon}|$ calculated is plotted for the associated temperature T, where curve sections indicated by arrows describe the range of heating. Obviously, within this range of heating considerably higher values of thermally induced strain-rates occur than is the case for cooling-down. The black dashed line labeled 'I' describes the temperature independent constant strain-rate as $\dot{\epsilon}_{\rm I}=0.05~\text{M/s}$. The temperature dependent strain-rate $\dot{\epsilon}_{\rm II}$, black

dashed line labeled 'II', is the result of a linear approximation of average strain-rates which occur within the HAZ during thermal welding cycles.

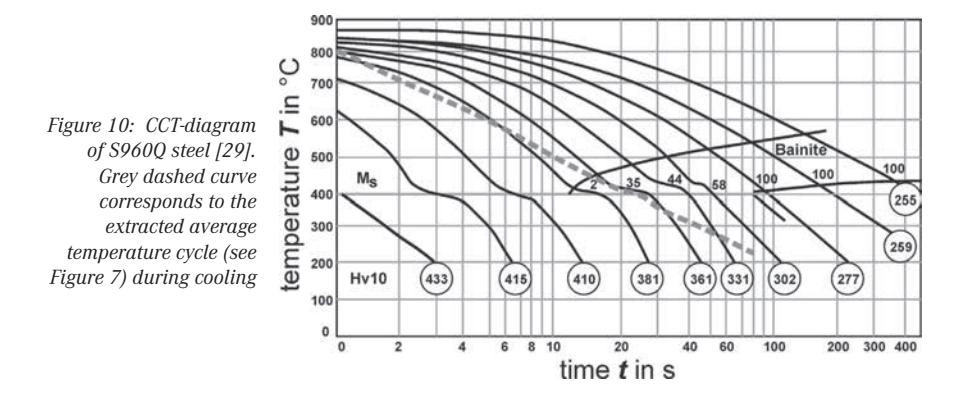
Experimental plan. To perform Gleeble®-experiments, an experimental plan must be designed where the solid phases, temperature ranges and strain-rates to be tested should be clarified. In Figure 10, the cooling down range of the average temperature cycle of the HAZ (see Figure 7) is drawn into a CCT-diagram for S960Q steel [29] by means of a grey dashed curve. The average temperature cycle at position B of Figure 9

crosses the region of austenite, bainite and martensite.

Therefore, with the intention of establishing a material database for numerical weld simulation by using S960QL steel, the temperature dependent stress-strain experiments will be conducted on the base material S960QL and on the related solid phases austenite, bainite and martensite. The resulting experimental plan with associate temperatures to be tested is given in Table 3. The transformation of the base material S960QL into the solid phases of bainite, martensite and austenite is based on the characteristics $\dot{T}_{heating}\text{, }t_{H}\text{, }T_{peak}$ and temperature evolution above 800 °C (see Figures 7, 8). To produce a bainitic microstructure, a temperature-rate of \dot{T} = -3 K/s during cooling from $800\,^{\circ}\text{C}$ to $300\,^{\circ}\text{C}$ was applied, which corresponds to a cooling time of $t_{8.5}$ = 100 s. The generation of the martensitic microstructure requires a temperature-rate of $\dot{T} = -50 \text{ K/s}$ equal to a cooling time of $t_{8.5} = 6$ s. These temperature-rates are appropriate to produce pure bainitic or pure martensitic microstructures, respectively (see Figure 10).

Furthermore, two experimental series with different strain-rates to be tested will be conducted using the experimental plan given by Table 3. The first experimental series deals with experiments at a constant slow strain-rate of $\dot{\epsilon}_{\rm I}$ = 0.05 %/s The second experimental series comprises stress-strain experiments with temperature dependent strain-rates from $\dot{\epsilon}_{\rm II}(T$ = 20 °C) = 0.1 %/s to $\dot{\epsilon}_{\rm II}(T$ = 1200 °C) = 1.5 %/s, which are derived by approximated strain-rates within the HAZ (see Figure 9).

Specimen geometry for Gleeble®-experiments. After clarifying the experi-



T in °C	25	100	200	300	400	500	600	700	800	900	1000	1100	1200
Base material	×	×	×	×	×	×	×	×					
Bainite	×	×	×	×	×	×	×						
Martensite	×	×	×	×	×	×	×	×					
Austenite							×	×	×	×	×	×	×
Strain rate $\dot{\epsilon}_{\rm I}$ (%/s)	0.05												
Strain rate $\dot{\epsilon}_{\rm II}$ (%/s)	0.1	0.19	0.31	0.43	0.55	0.67	0.79	0.91	1.03	1.14	1.26	1.38	1.5

Table 3: Experimental plan for temperatures, solid phases and strain-rates (see Figure 9) to be tested

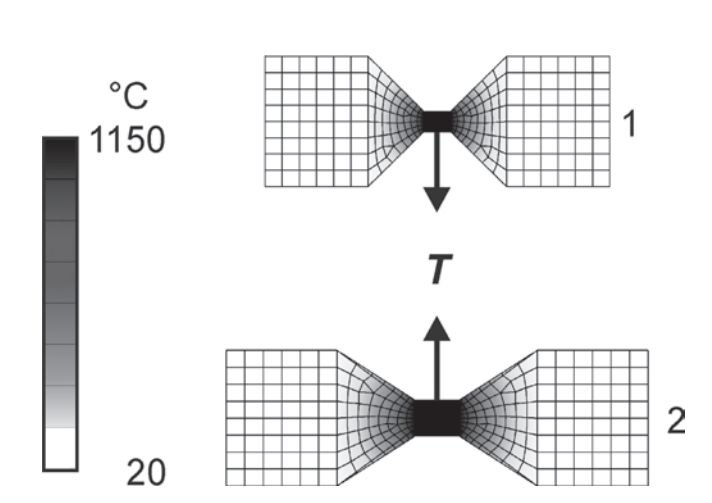


Figure 11: Contour plot of stationary temperature field for two different specimen geometries calculated by FEA

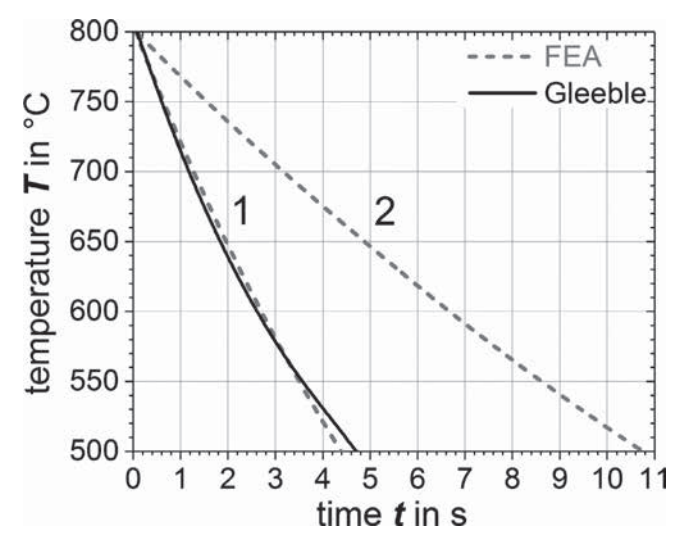


Figure 12: Thermal cycles during passive cooling of specimen geometries "1" and "2" (see Figure 11). Grey dashed curve – numerically calculated, Black curve – Gleeble®-experiment

mental plan, the specimen geometry for experiments using the Gleeble®3500-test system has to be designed. The specimens are machined from sheets of S960QL steel with a maximum thickness of 6 mm. The experiments are restricted to the passive cooling of the specimens, which is advantageous for getting a better uniformly heated cross-section of the specimens. To achieve this, possible specimen geometries are tested by 3D numerical simulation (SYS-WELD®) to ensure minimum cooling rates which are necessary for producing a pure solid phase of martensite in the middle of the specimens. In Figure 11, two different specimen geometries with a thickness of 5.5 mm are shown exemplarily. The thermal boundary conditions within numerical simulation were derived from thermal boundary conditions approximated by the Gleeble®3500-test system. The middle of the flat specimens were thermally loaded until a nearly stationary temperature field was attained, which is shown on the contour plot in Figure 11. Subsequently, thermal loading was stopped and the specimens were cooled down passively via unforced heat transfer through convection, radiation and conduction. Sections of the resulting thermal cycles while temperatures dropped from 800 °C to 500 °C are plotted by the grey dashed curves in Figure 12. For specimen "1" (see Figure 11) a cooling time of $t_{8.5} \approx 4.4 \text{ s}$ and for specimen "2" (see Figure 11) a cooling time of $t_{8.5} \approx 10.9 \text{ s were calculated.}$ The full black curve in Figure 12 represents a section of a thermal cycle measured during Gleeble®experiments by using specimen geometry "1", in which the specimen was cooled passively and reached a cooling time of $t_{8,5} \approx 4.7 \text{ s.}$

Comparing a CCT-diagram for S960Q steel (see Figure 10) with thermal cycles presented in Figure 12, the assumption can be made that using specimen geometry "1" for Gleeble®-experiments enables the production of pure martensitic phases. Following this condition and for reasons of comparability flat specimen geometry "1" was used for

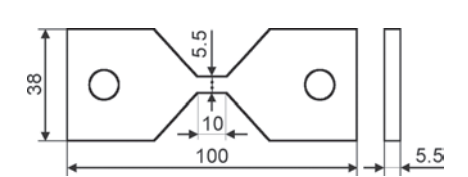


Figure 13: Flat specimen geometry "1". (see Figure 11) Measuring range is located at the middle of the flat bridge, where thermocouples are tack welded for recording temperature signal.

all stress-strain experiments. The dimension of specimen "1" is given in Figure 13.

Strain-rate controlled determination of stress-strain behavior. The main focus of this present work is the strain-rate controlled determination of temperature dependent stress-strain behavior of S960QL steel with related solid phases. Using the Gleeble®-test system, three different methods are possible to carry out stress-strain experiments. First, two simple methods not appropriate to perform strain-rate controlled experiments will be presented and discussed briefly. Then, the transversal strain-rate controlled method used for stress-strain experiments will be described in detail. All methods are exemplarily explained regarding the experimental procedures needed to determine the tensile stress-strain behavior for the heated base material S960QL at a temperature of T = 600 °C with predefined longitudinal strain-rate $\dot{\epsilon}_{long}$ = 0.05 %/s. However, all methods in the experimental procedure share the following points:

 The specimen was clamped into two electrically conductive clamping chucks by fixing bolts connected to the holes (see Figure 14) in the specimen.

- The specimen was heated using alternating current. Therefore, the required temperature was adjusted by machine-internal control of the electrical potential between the clamping chucks.
- The force application on the specimen is enabled by force transmission due to the fixing bolts inserted in the holes (see Figure 14).
- A heated specimen exhibits symmetric, but non-uniform temperature distribution in the axial direction, where the maximum temperature is located in the middle of the flat bridge (see Figure 15b).
- Thermocouples are tack welded at the middle of the flat bridge, where maximum temperature is expected (see Figure 14).
- The stress to be measured is evaluated by the force applied in relation to the actual cross-sectional area on the position of the tack welded thermocouples.
- The actual cross-sectional area is determined by the use of a C-gauge (strain crosswise transducer Type LVDT), which measures the transversal length of the flat bridge. The moveable thrust rod of the C-gauge type LVDT was modified by heat-resistant tape and oil to improve measurement accuracy of one or-

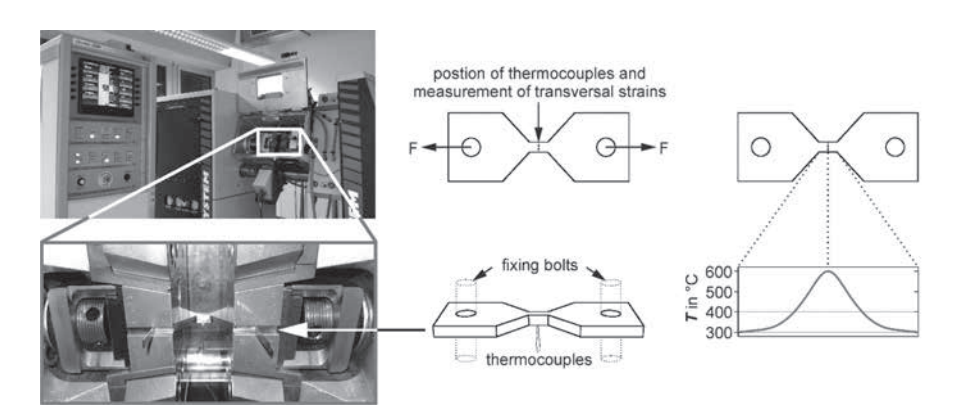


Figure 14: Gleeble® 3500 system with clamped specimen (IWF - Otto von Guericke University). Zoomed part of the measurement chamber, where the specimen (see Figure 1) to be tested is clamped into the two electrically conductive clamping chucks.

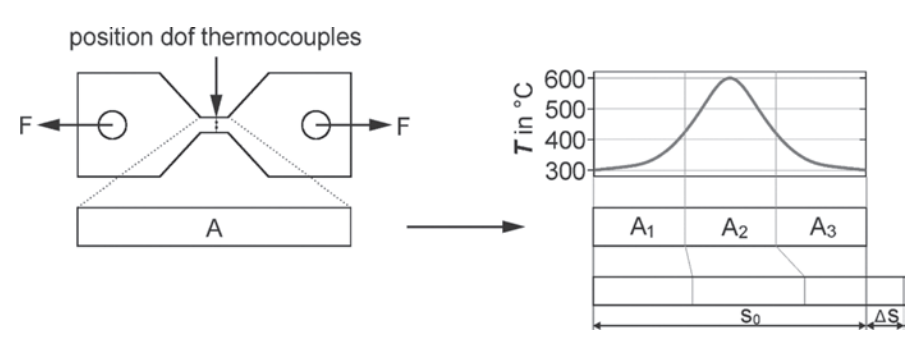


Figure 15: Non-uniform temperature distribution in the range of the flat bridge of the specimen. left - covered measuring range "A" by use of a L-gauge. right - resulting change Δs of the axial length s^0 as sum of the regions " A_1 ", " A_2 " and " A_3 "

der of magnitude to $\pm 1 \times 10^{-3}$ mm. Additionally, to prevent the measuring device from heating up by radiation, a sheet of high reflecting metal foil was used.

 Before conducting the experiments, the measurement chamber with the specimen already installed was evacuated twice and subsequently filled with the inert gas argon.

Strain-rate uncontrolled methods. The first method deals with the user defined change of the axial length per time unit of the flat bridge section to determine the stress-strain behavior. This means that the applied force will be increased until the pre-defined change of the axial length per time unit is reached. For this, an L-gauge is connected, for example, over the region "A" (see Figure 15a). The resulting transversal strain and thus the actual cross-sectional area can be measured by

the use of a C-gauge located at the middle of the flat bridge where the thermocouples are tack welded. Dictated by operational conditions, temperature distribution along axial direction is non-stationary, unknown to the experimenters and non-uniform (see Figure 15b). The latter is the reason why the controlled change of the axial length Δs by the use of an Lgauge is a sum of the single changes in length of sections "A1", "A2" and "A3" which have different average temperatures among themselves. In connection with the (unknown) temperature dependent stress-strain behavior of the material tested, the strain-rate for the position exhibiting the maximum temperature measured cannot be preadjusted by the experimenters.

Secondly, a force-rate control method is described. Here, the specimen is instilled

with a predefined constant force increase per time unit. Because of the unknown stress-strain behavior, a constant force increase per time unit seems to be the first appropriate approach. In this way, a stress-strain curve can be evaluated. Now, the consequences of the resulting strain-rates will be exemplarily explained on a hot tensile curve for the base material S960QL at an elevated temperature $T = 600~\rm C$ (see Figure 16), which has been taken from the results of this study (see Figures 23-25, Table 5).

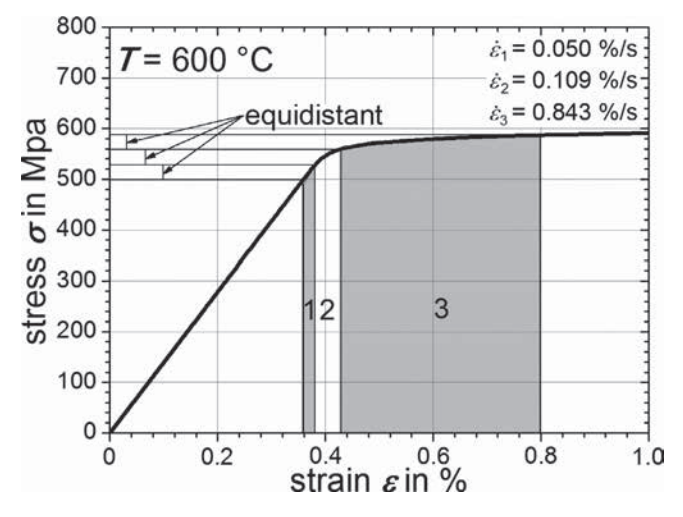
The hot tensile curve (see Figure 16) is characterized by a region of pure elastic behavior, a transition region of elastic-plastic behavior and a region of pure plastic behavior. Assuming an equidistant increase in stress (force) per time unit leads to strains indicated by sections 1-pure elastic, 2-transition from elastic to plastic and 3-pure plastic. For section 1, the increase in force per time step results in an increase of stress with $\Delta \sigma \approx +130$ MPa. Due to the time step chosen which is needed for applying force, the longitudinal strain-rate for section 1 is $\dot{\epsilon}_1 = 0.050 \text{ %/s}$. The same load step and time step needed for section 2 and for section 3 leads to an enhanced longitudinal strain-rate of $\dot{\epsilon}_2$ = 0.109 %/s \approx 2.2 \times $\dot{\epsilon}_1$ and $\dot{\varepsilon}_3 = 0.873 \text{ %/s} \approx 16.9 \times \dot{\varepsilon}_1.$

To sum it up: for the exemplarily evaluated stress-strain curve of base material S960QL at a temperature of $T=600\,^{\circ}\text{C}$ the strain-rates between elastic region 1 and plastic region 3 differ by 16.9 times. Obviously, the force-rate controlled method is not appropriate for carrying out stress-strain experiments while maintaining nearly constant strain-rates for each characteristic part of the stress-strain curve.

Transversal strain-rate controlled method. As a next step, the transversal strain-rate controlled method used for stress-strain experiments of this study will be explained in detail. Its main feature is to control longitudinal strain ϵ_{long} by means of transversal strain ϵ_{trans} or in this way the associated strain-rates, respectively. The fundamental basis for this is a correlation between longitudinal and transversal strains during a tensile test, which is given in the definition of the Poisson's ratio ν (see Equation 3). The correlation between the strain-rates $\dot{\epsilon}_{long}$ and $\dot{\epsilon}_{trans}$ can be derived by application of the total time derivation on the definition of the Poisson's-ratio:

$$v = \frac{\varepsilon_{trans}}{\varepsilon_{long}} = \left| \frac{d(...)}{dt} \right|$$

Figure 16: Change in strain-rates by applying the force-rate controlled method, explained on a tensile curve given by results of this study (see Figures 23-25, Table 5). Material behavior of the sections: 1-elasitc, 2-elastic-plastic, 3-plastic



T (°C)	25	100	200	300	400	500	600	700	800	900	1000	1100	1200
$\nu_{\rm elastic}$	0.298	0.302	0.307	0.312	0.317	0.322	0.328	0.333	0.338	0.343	0.348	0.353	0.358
ν_{plastic}	0.5												

 $\it Table~4: Temperature~dependent~Poisson's-ratio~v~for~S960QL~steel~determined~by~in-house~experiments~using~the~resonance-method$

Table 5: Ramberg-Osgood-parameters to describe stress-strain curves for the base material

T (°C)	E	R _e (N	MPa)	R _{p,0.2}	(MPa)	n		
T (°C)	(GPa)	$\boldsymbol{\dot{\epsilon}}_{I}$	$\boldsymbol{\dot{\epsilon}_{II}}$	$\boldsymbol{\dot{\epsilon}_{I}}$	$\dot{\epsilon}_{\rm II}$	$\boldsymbol{\dot{\epsilon}_{I}}$	$\dot{\epsilon}_{\rm II}$	
25	211	860	/	1040	/	29	/	
100	207	825	/	980	/	25.7	/	
200	200	800	/	935	/	23.5	/	
300	192	770	/	900	/	23.8	/	
400	184	730	743	861	877	25	24.6	
500	171	670	695	788	800	37	32	
600	160	521	636	582	682	55	80	
700	144	222	358	254	385	47	80	

with
$$v \neq f(t) \rightarrow \dot{\epsilon}_{long} = \frac{1}{v} \dot{\epsilon}_{trans}$$

 ϵ_{long} – longitudinal strain; $\dot{\epsilon}_{long}$ – longitudinal strain-rate; ϵ_{trans} – transversal strain; $\dot{\epsilon}_{trans}$ – transversal strain-rate; ν – Poisson's ratio

(3)

Now, the required longitudinal strainrate will be transferred into the required transversal length change of the cross-section of the flat bridge ΔC per time step Δt . For this, the change of transversal strain $\Delta \epsilon_{trans}$ is mathematically formulated by use of the relations given in Figures 17 and 18:

with
$$\Delta C = C - C_0 - \Delta C_{th} \rightarrow$$

$$\Delta \dot{\varepsilon}_{\text{trans}} \cdot \frac{1}{\Delta t} = \frac{\Delta C}{(C_0 + \Delta C_{\text{th}})} \cdot \frac{1}{\Delta t}$$
 (4)

C – transversal length under applied load; C_0 – transversal length at room temperature; – transversal length change; ΔC_{th} – thermal transversal length change; $\Delta \epsilon_{trans}$ – change of transversal strain; Δt – time step

Inserting Equation 4 into the relation given by Equation 3 and transposing to time step leads to Equation 5:

 $\Delta\epsilon_{long}$ – change of longitudinal strain

Using the mathematical formulation presented in Equation 5, the experimenter is able to plan strain-rate controlled stress-strain experiments. Inserting the desired longitudinal strain-rate (see Table 3), Poisson's-ratio (see Table 4) and a transversal length change ΔC defined by the experimenter leads to the required time step Δt . Subsequently, the experimenter has to incorporate ΔC and Δt into the programming guidelines for the Gleeble®-experiments where ΔC will be measured by the use of a C-gauge clamped to the flat bridge of the specimen.

The stress-strain experiments will be divided into two consecutive steps. First, a pure elastic material behavior is assumed. For this, the transversal length change is set to $\Delta C_{elastic}$ = –0.04 mm which will guar-

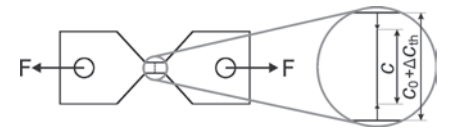


Figure 17 Required relations related to the side length of the quadratic cross-section of the flat bridge. C_0 – length at room temperature, $\Delta C_{\rm th}$ – thermal length change (see Figure 18, C – length under applied load (force)

antee covering the region for elastic material behavior. This change of length together with $\nu_{elastic}$ (see Table 4) will be considered in executing the first experimental step. After reaching $\Delta C_{elastic}$ = -0.04 mm by performing the tensile test, the second experimental step is performed where pure plastic material behavior is expected. Here, $\Delta C_{plastic}$ will be newly specified as $\Delta C_{plastic}$ = -0.13 mm. The latter in connection with $\nu_{plastic}$ (see Table 4) will be considered when performing the second experimental step.

Evaluation of Gleeble®-experiments. Because of the method chosen to perform the stress-strain experiments according to the transversal strain-rate method, the results should be evaluated as shown below. Initially, stress-strain curves have to be composed. Then, the resulting strain-rates must be verified. Finally, the measured stress-strain curves will be approximated by material law. These steps are exemplarily, explained in a tensile test for the base material S960QL heated to a temperature of T = 600 °C, where the predefined magnitude of the longitudinal strain-rate is set to $\dot{\epsilon}_{long}$ = 0.05 %/s.

Composition of stress-strain curves. The measured values of the transversal length change ΔC and the applied force F as well as the given values for transversal length at room temperature C_0 (see Figure 13) and the thermal transversal length change ΔC_{th} (see Figure 18) serve to calculate the associated longitudinal strain ϵ_{long}

and stress $\sigma_{\text{true}}.$ The true stress is calculated by Equation 6:

$$\sigma_{\text{true}} = \frac{F}{\left(C_0 + \Delta C_{th} + \Delta C\right)^2} \tag{6}$$

F – applied force by the Gleeble®-test system; σ_{true} – true stress

Subsequently, the associated longitudi $_{ong}$ will be calculated in Equation 7 by means of the elastic and plastic Poisson's-coefficient (see Table 4) and then transferred into the true longitudinal strain $\epsilon_{long,}$ $_{true}$ (see Equation 8):

$$\varepsilon_{\text{long,i}} = -\frac{1}{v_{i}} \cdot \frac{\Delta C}{(C_{0} + \Delta C_{th})}$$
(7)

with $i := \{elastic; plastic\}$

$$\varepsilon_{\text{long, true}} = \ln(1 + \varepsilon_{\text{long, i}})$$
 (8)

 $\epsilon_{long,\,true}$ – true longitudinal strain

The resulting stress-strain curves are plotted in Figure 19a where the black curve was calculated using the elastic Poisson's-coefficient $\nu_{\rm elastic}$ and the grey curve results by applying the plastic Poisson's-coefficient $\nu_{\rm plastic}$. Finally, the stress-strain curve required has to be composed from parts of the elastic and plastic stress-strain curves (see Figure 19a). For this purpose, the yield stress of the plastic stress-strain curve (grey) must be identified by finding the transition point at which the slope of

$$\text{with } \dot{\epsilon}_{trans} \approx \frac{\epsilon_{trans}}{\Delta t} \text{ and } \dot{\epsilon}_{long} \approx \frac{\epsilon_{long}}{\Delta t} \rightarrow \frac{\epsilon_{long}}{\Delta t} = -\frac{1}{\nu} \cdot \frac{\Delta C}{(C_{_0} + \Delta C_{_{th}}) \cdot \Delta t} \rightarrow \Delta t = \frac{\Delta C}{\nu \cdot \frac{\epsilon_{long}}{\Delta t} \cdot (C_{_0} + \Delta C_{_{th}})}$$

Equation 5

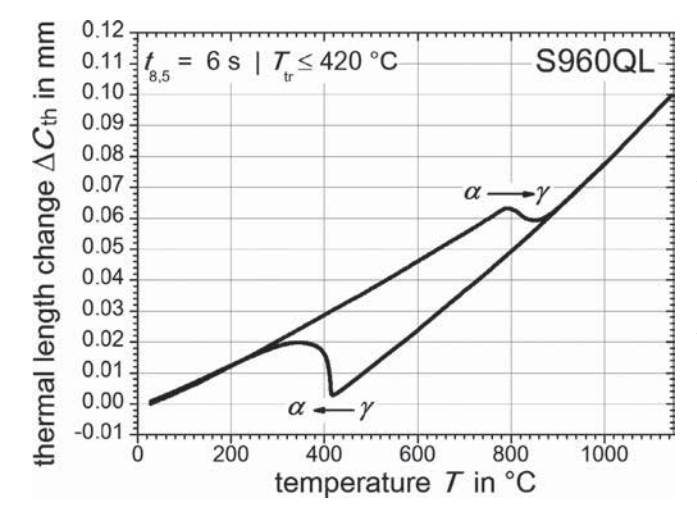
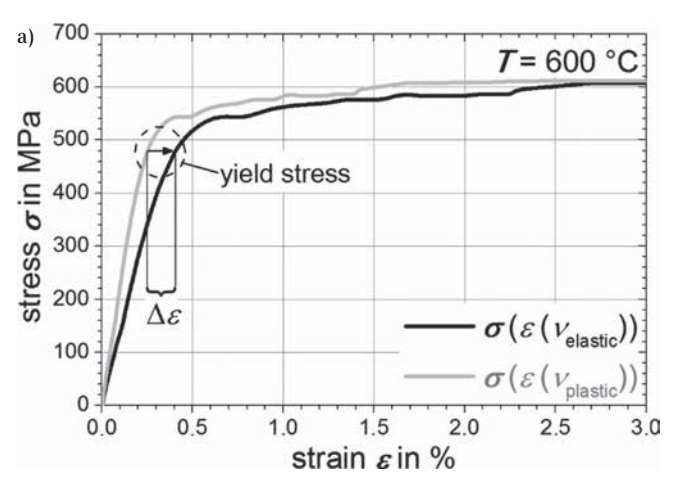


Figure 18: Dilatometric curve of S960QL steel measured by Gleeble-experiments using characteristics of average temperature cycle (see Figure 8), Martensit start temperature S = 420 °C



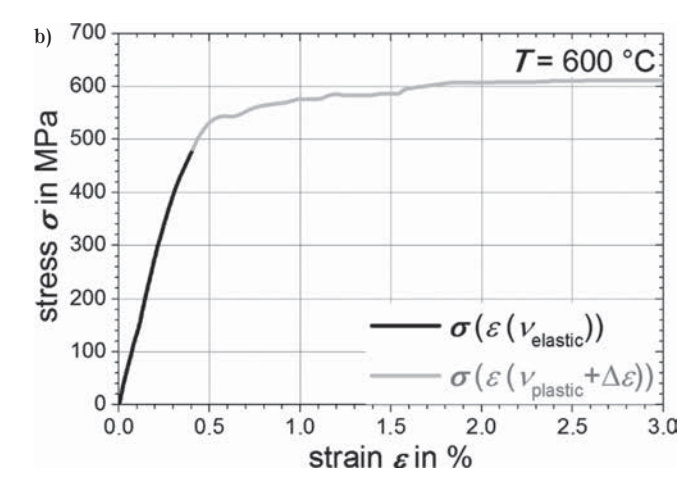


Figure 19: a) Stress-strain curves calculated by use of the elastic Poisson's-coefficient $v_{elastic}$ (black curve) or plastic Poisson's-coefficient $v_{plastic}$ (grey curve), respectively; b) Composed stress-strain curve

the hot tensile curve changes from linear to non-linear behavior. Then, the part of the stress-strain curve (grey) above the yield stress will be shifted by towards the elastic stress-strain curve (black). Doing this, the required stress-strain curve is composed as shown in Figure 19b. This above-described method will be used to evaluate all other stress-strain experiments performed within this study.

Verification of strain-rates. After the required stress-strain curves have been composed, the resulting strain-rates must be verified. Corresponding to the exemplarily case examined for the base material at $T=600\,^{\circ}\text{C}$, a magnitude of the longitudinal strain-rate at $\dot{\epsilon}_{long} \approx 0.05\,\text{\%/s}$ should be achieved. The transversal length change measured by the C-gauge is presented in Figure 20. According to Figure 19a, plastic stress-strain behavior can be derived for regions II and III. Evaluating the average slope $\Delta C/\Delta t$ for regions II and III and applying

Equation 5 with $\nu_{plastic}$ (see Table 4), leads to the resulting longitudinal strain-rates of $\dot{\epsilon}_{region\,II}\approx 0.031$ %/s and $\dot{\epsilon}_{region\,III}\approx 0.031$ %/s. The deviation between the resulting strain-rate of region II as compared to the planned strain-rate can be explained by the approach of the transversal strain-rate method for region II. Here, the experiment was designed using the elastic Poisson's-coefficient , but the real material behavior in region II exhibits plastic flow. At $\nu_{elastic} < \nu_{plastic}$ for all temperatures, the resulting (plastic) strain-rate must be lower than the planned (elastic) strain-rate (see Equation 5).

Because of the measurement uncertainty of the C-gauge, the slope $\Delta C/\Delta t$ can hardly be evaluated for elastic region I. Therefore,

the definition of Young's-modulus is used to assess the resulting longitudinal strain-rate (see Equation 9). Applying the total time derivation to the definition of E and assuming a constant behavior and a nearly constant cross-sectional area within elastic region I, the longitudinal strain rate $\dot{\epsilon}_{region\,I}$ can be assessed as follow:

A – cross-sectional area of the flat bridge; E – Young's-modulus; F – applied force by the Gleeble®-test system; \dot{F} – applied force-rate of the Gleeble®-test system; $\epsilon_{region\,I}$ – longitudinal strain of region I; $\dot{\epsilon}_{region\,I}$ – longitudinal strain-rate of region I; $\sigma_{region\,I}$ – stress of region I

$$\sigma_{\text{region,I}} = E \cdot \epsilon_{\text{region,I}} \left| \frac{d(...)}{dt} \text{ with } \sigma_{\text{E}} = \frac{F}{A} \text{ and } E = E_{\text{const}}; A = A_{\text{const}} \rightarrow \epsilon_{\text{region,I}} \approx \frac{\dot{F}}{A_{\text{const}} \cdot E_{\text{const}}} = \frac{\dot{F}}{(C_0 + \Delta C_{\text{th}})^2 \cdot E$$

Equation 9

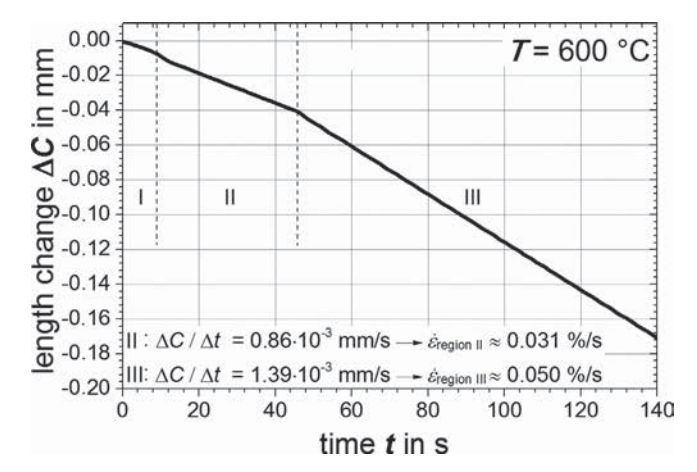


Figure 20: Transversal length change measured by the C-gauge. Applying average slope of $\Delta C/\Delta t$ on Eq.5 leads to the resulting longitudinal strain rates for plastic regions II and III

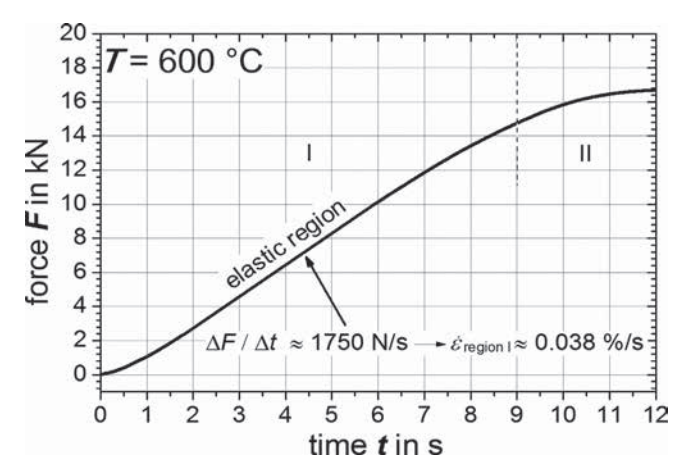


Figure 21: Applied force within elastic region I. Applying average slope $\Delta F/\Delta t$ on Equation 9 leads to resulting longitudinal strain-rates for elastic region I.

Evaluating the average slope $\Delta F/\Delta t$ for elastic region I (see Figure 21) and applying Equation 9 with $\Delta C/\Delta t \approx \dot{F}$ and E(T = 600 °C) (see Table 5), leads to a resulting longitudinal strain-rate of $\dot{\epsilon}_{\rm region~I} \approx 0.038$ %/s, which is slightly below the planned strain-rate of $\dot{\epsilon}_{\rm long} \approx 0.05$ %/s. Because of the inherent working principle of the Gleeble®-test system during the machine startup, this result seems to be reasonable. Here, the controlalgorithm during the machine startup in combination with the small strain-range within elastic region I lead to lower strains per time step and thus to strain-rates lower than planned.

Finally, the strain-rate dependent stress-strain experiment for the base material S960OL at a temperature of T = 600 °C was planned to achieve a magnitude of the longitudinal strain-rate with $\dot{\epsilon}_{long} \approx 0.05$ %/s. Executing the stress-strain experiments by means of the transversal strain-rate controlled method, results in longitudinal strain-rates of $\dot{\epsilon}_{region~II} \approx 0.038$ %/s for elastic region I (see Figures 20, 21), $\dot{\epsilon}_{region~III} \approx 0.031$ %/s for the first plastic region II (see Figure 20) $\dot{\epsilon}_{region~IIII} \approx 0.050$ %/s and for the second plastic region

III. In this manner, the transversal strainrate controlled method seems to be appropriate for carrying out stress-strain experiments by ensuring compliance with the predefined magnitude of longitudinal strain-rates.

Approximation of the composed stressstrain curves. For the case examined, the verified strain-rates for region I and region II (see Figure 22) are below the predefined strain-rate (see Figures 20 and 21). Therefore, the first part of the composed stressstrain curve exhibits lower yield-stress and a lower stress level of plastic flow compared to the enhanced planned strain-rate, which could be attained experimentally within region III (see Figure 20). Thus, the composed stress-strain curve (see Figure 19b) does not fully reflect the stress-strain behavior as expected for experiments exhibiting a constant longitudinal strain-rate 0.05 %/s. In order to derive a stress-strain curve in accordance with a strain-rate of 0.05 %/s, the required stress-strain curve must be approximated by the Ramberg-Osgood-relationship [30], which is rendered in a rewritten formulation in Equation 10. The fixed parameters are the stress σ and the temperature dependent Young's-modulus E, whereas the fit-parameters are the yield stress at 0.2 % plastic strain $R_{\rm p0.2}$ and the correlation coefficient .

$$\varepsilon_{\text{long}} = \frac{\sigma}{E} + 0.002 \cdot \left(\frac{\sigma}{R_{\text{p,0.2}}}\right)^{\text{n}} \tag{10}$$

 ϵ_{long} – longitudinal strain; σ – stress; $R_{p0.2}$ – yield stress at 0.2 % plastic strain; E – Young's-modulus; n – correlation coefficient

The fit-parameters must be selected in such a way that within regions I and II the resulting stress-strain curve lies above the composed stress-strain curve. Additionally, the resulting stress-strain curve has to be in accordance with the composed stress-strain curve within region III where the planned strain-rate of 0.05 %/s was reached. By using Young's-modulus $E(T=600~{\rm ^{\circ}C})=160~{\rm MPa}$ (see Table 5) and in compliance with the aforementioned conditions, the associated fit-parameters are $R_{\rm p0.2}=160~{\rm MPa}$ and n = 55. The resulting approximated stress-strain curve using the Ramberg-Osgood-relationship is given

T (°C)	Е	R _e (N	МРа)	R _{p,0.2}	(MPa)	n		
T (°C)	(GPa)	$\dot{\epsilon}_{_{\mathrm{I}}}$ $\dot{\epsilon}_{_{\mathrm{II}}}$		ŧ _Ι	$\boldsymbol{\dot{\epsilon}_{II}}$	$\boldsymbol{\dot{\epsilon}_{I}}$	$\dot{\epsilon}_{\rm II}$	
25	211	635	/	845	/	14.4	/	
100	207	616	/	820	/	14.5	/	
200	200	600	/	800	/	14.6	/	
300	192	578	/	775	/	15	/	
400	184	555	600	760	774	20	19	
500	171	510	553	697	720	24.5	23.5	
600	160	462	504	535	585	32	34	

Table 6: Ramberg-Osgood-parameters to describe stress-strain curves for solid phase bainite

T (9C)	Е	R _e (N	MPa)	R _{p,0.2}	(MPa)	n		
T (°C)	(GPa)	ŧι	ŧ _{II}	ŧι	ŧ _{II}	ŧι	ĖΠ	
25	211	1070	/	1250	/	11	/	
100	207	1048	/	1210	/	10.7	/	
200	200	1005	/	1180	/	11.5	/	
300	192	967	/	1155	/	14.5	/	
400	184	871	899	1028	1058	35	33	
500	171	700	755	808	864	33	37	
600	160	487	573	546	645	30	37	
700	144	233	353	263	392	45	45	

Table 7: Ramberg-Osgood-parameters to describe stress-strain curves for solid phase martensite

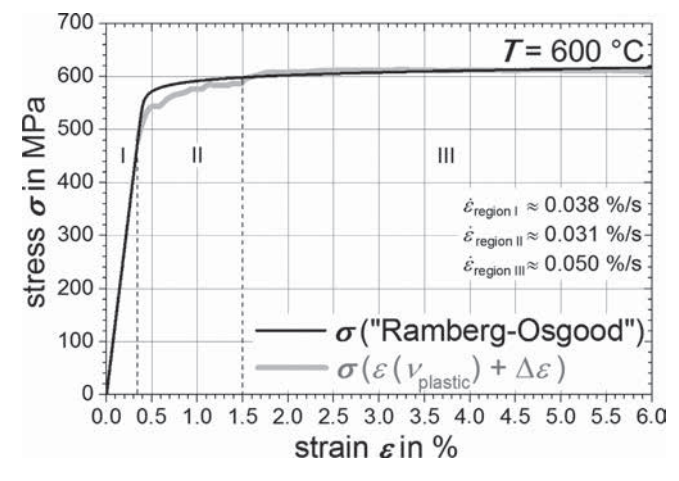


Figure 22: Approximated stress-strain curve (black) by use of the Ramberg-Osgood-relationship (see Equation 10) [30]

T (9C)	E	$R_{\rm e}$ (N	MPa)	$R_{p,0.2}$	(MPa)	n		
T (°C)	(GPa)	ŧι	ĖΠ	ŧι	ŧ _{II}	ŧι	ĖΠ	
600	160	60.7	65	105	107	4.7	4.5	
700	144	54.4	60	99	103	5.2	5	
800	128	43.8	50	85	95	7	5.8	
900	111	28.9	35	65	72	9	6.5	
1000	100	25.3	31.5	51	60	9.3	8	
1100	90	22.8	28.5	43	51	11	10	
1200	80	20.2	25	38	46	12	11	

Table 8: Ramberg-Osgood-parameters to describe stress-strain curves for solid phase austenite

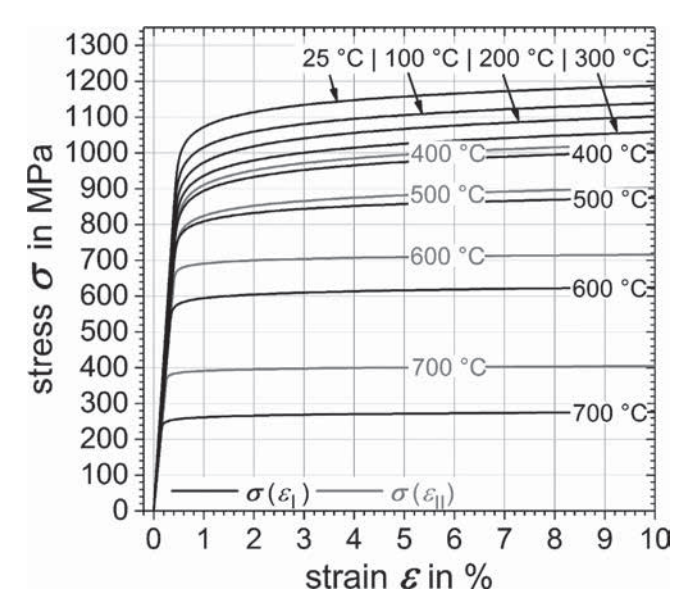


Figure 23: Resulting stress-strain curves for the base material by applying the Ramberg-Osgood-relationship (see Equation 10) using paramters given in Table 5

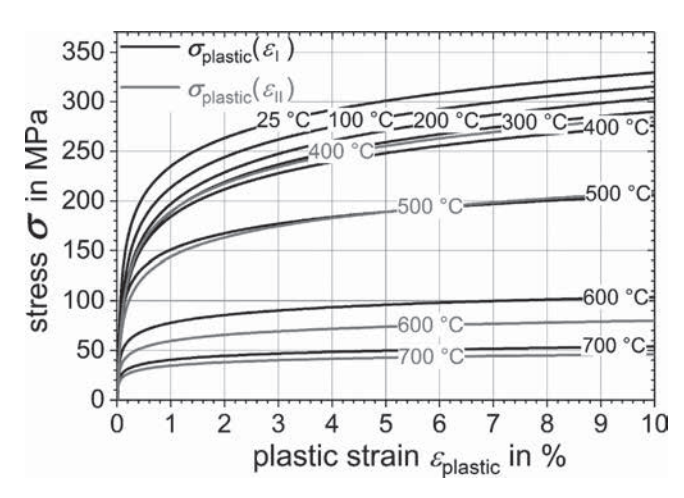


Figure 25: Derived slopes of plastic flow by means of the Ramberg-Osgoodrelationship (see Equation 10) using parameters in Table 5

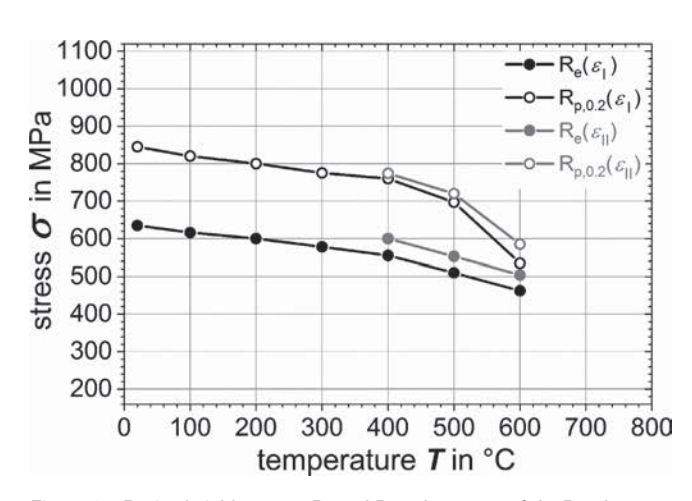


Figure 27: Derived yield stresses R_e and $R_{p,0.2}$ by means of the Ramberg-Osgood-relationship (see Equation 10) using parameters in Table 6

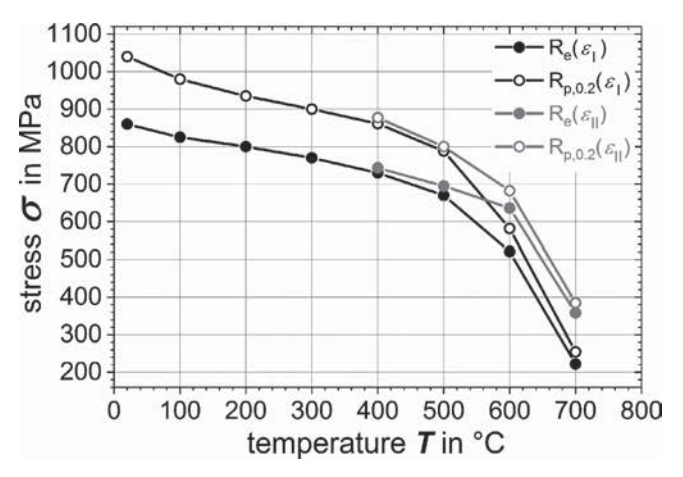


Figure 24: Derived yield stresses R_e and $R_{p,0.2}$ by means of the Ramberg-Osgood-relationship (see Equation 10) using parameters of Table 5

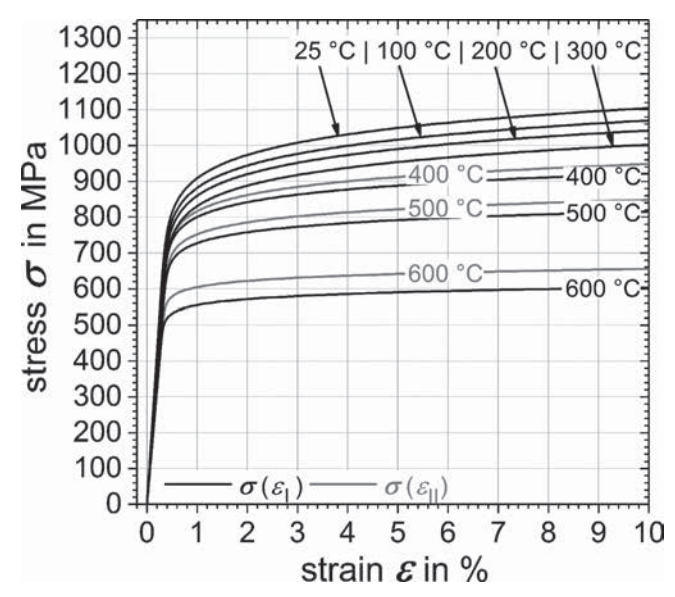


Figure 26: Resulting stress-strain curves for the solid phase bainite by applying the Ramberg-Osgood-relationship (see Equation 10) using paramters given in Table 6

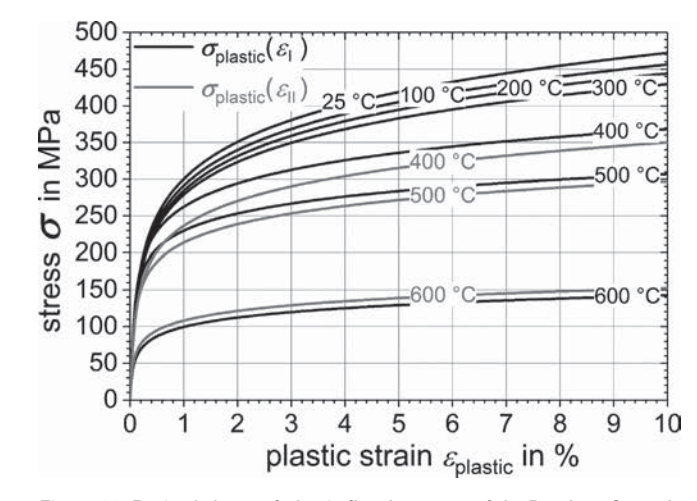


Figure 28: Derived slopes of plastic flow by means of the Ramberg-Osgoodrelationship (see Equation 10) using parameters in Table 6

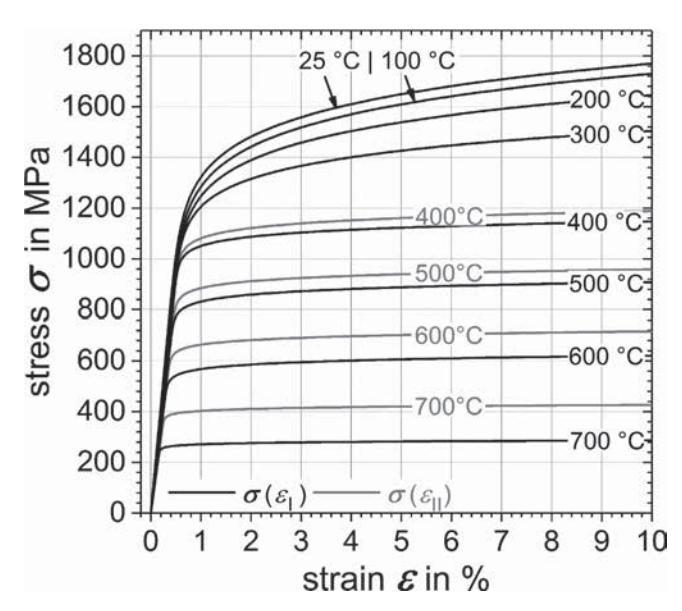


Figure 29: Resulting stress-strain curves for the solid phase martensite by applying the Ramberg-Osgood-relationship (see Equation 10) using paramters given in Table 7

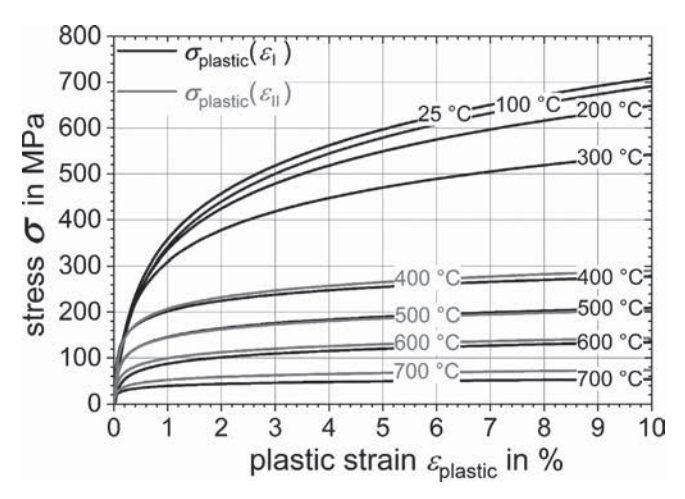


Figure 31: Derived slopes of plastic flow by means of the Ramberg-Osgood-relationship (see Equation 10) using parameters in Table 7

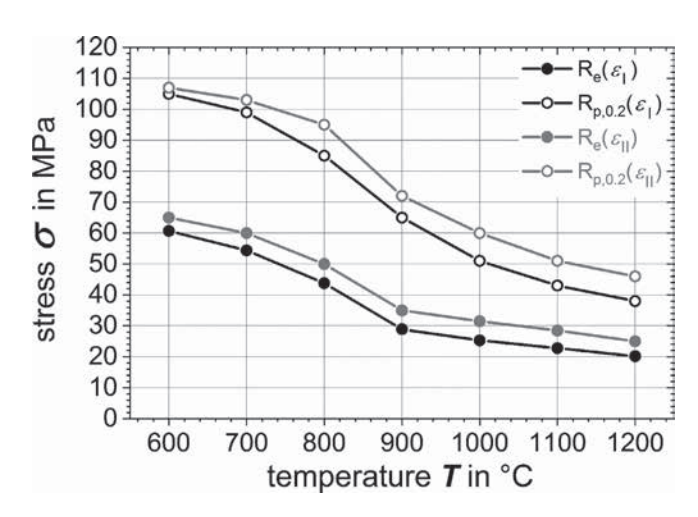


Figure 33: Derived yield stresses R_e and $R_{p,0.2}$ by means of the Ramberg-Osgood-relationship (see Equation 10) using parameters in Table 8

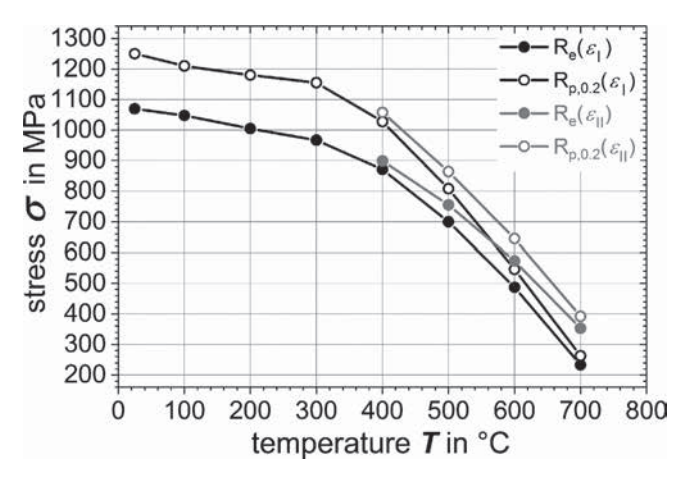


Figure 30: Derived yield stresses R_e and $R_{p,0.2}$ by means of the Ramberg-Osgood-relationship (see Equation 10) using parameters in Table 7

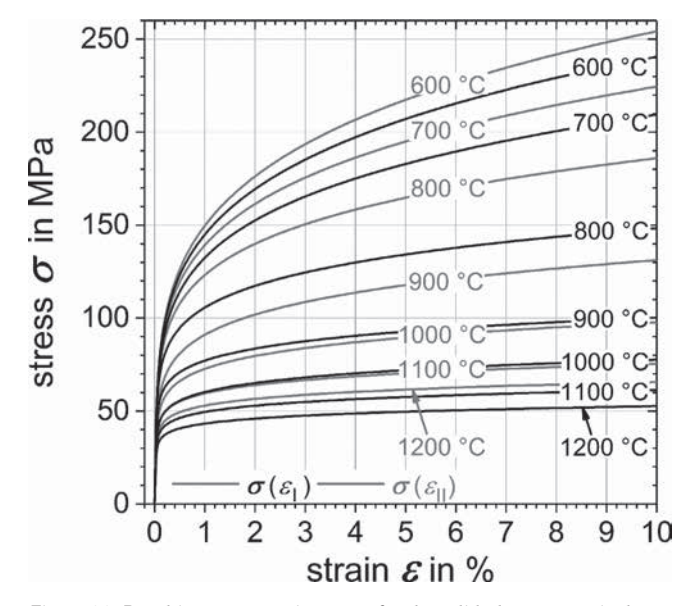


Figure 32: Resulting stress-strain curves for the solid phase austenite by applying the Ramberg-Osgood-relationship (see Equation 10) using paramters given in Table 8

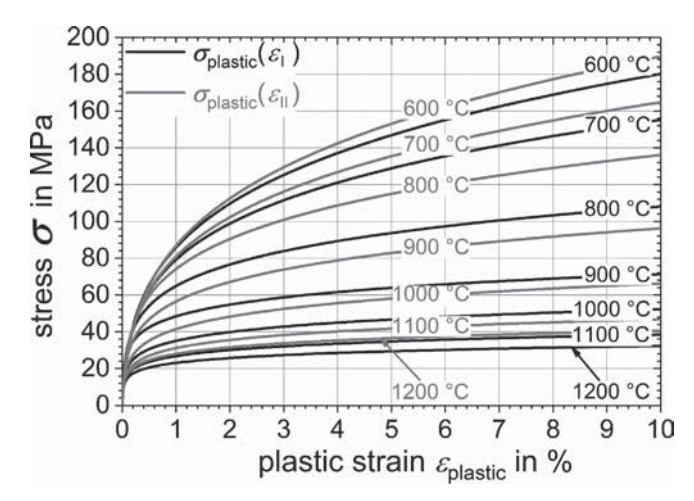


Figure 34: Derived slopes of plastic flow by means of the Ramberg-Osgoodrelationship (see Equation 10) using parameters in Table 8

in Figure 22 and shows the stress-strain behavior expected for a longitudinal strain-rate of $\dot{\epsilon}_{long} \approx 0.05$ %/s.

The design of the Gleeble®-experiments in combination with the methods for the evaluation of the Gleeble®-experiments will be applied for all temperature and strain-rate dependent stress-strain experiments within this study. The stress-strain experiments for each temperature and strain-rate will be repeated twice.

Results and discussion

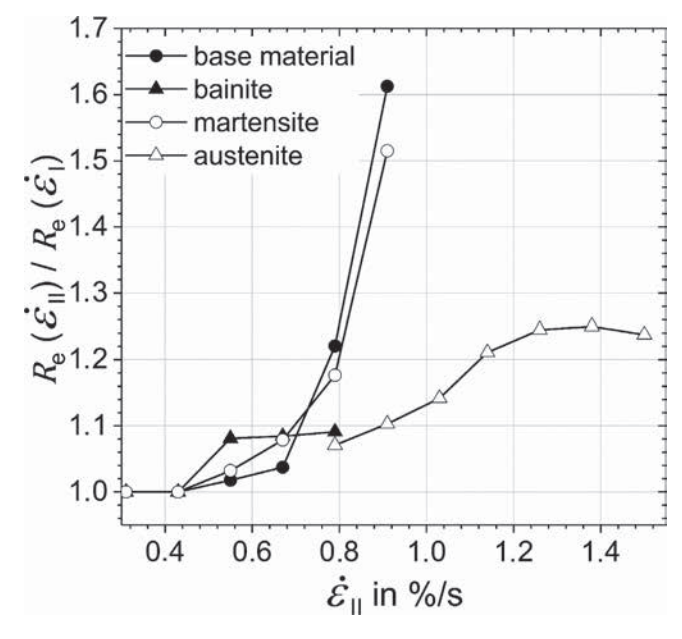
The following results are based on strainrate controlled stress-strain experiments performed using the Gleeble®3500-test system. In this context, the transformable HSLA steel S960QL and related solid phases were characterized by temperature dependent hot tensile tests (see Table 3) applying various strain-rates $\dot{\epsilon}_{_{\rm I}}$ and $\dot{\epsilon}_{_{\rm II}}$ (see Table 3). The experimental procedure and the evaluation method are described in the sections above. In Tables 5-8, the Ramberg-Osgood-parameters needed for a description of stress-strain curves are given (see Equation 10). The resulting temperature dependent stress-strain curves, yield stresses and slopes of plastic flow are presented in Figures 23 to 34. In Figures 35, 36 the strain-rate influence on yield stress is shown, where normalizing $Re(\dot{\epsilon}_{II})$ and Rp,0.2($\dot{\epsilon}_{II}$) is done by reference values of $Re(\dot{\epsilon}_{l})$ and $Rp0.2(\dot{\epsilon}_{l})$, respectively. Here, strain-rate is linear, increasing with temperature according to Table 3.

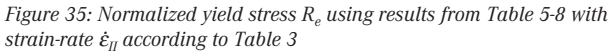
Using the Gleeble®-test system to determine the strain-rate dependent stressstrain behavior of metals, the longitudinal strain-rate at peak-temperature positions can be controlled by the predefinition of the associated transversal strain-rate applying Poisson's-ratio. To obtain stressstrain curves which fully reflect the stressstrain behavior for the intended strain-rate, the composed stress-strain curve (see Figure 19b) must be approximated by the appropriate material-law, for example by the Ramberg-Osgood-relationship (see Equation 10). With respect to future investigations, experimenters should choose a minor transversal length change $\Delta C_{\text{elastic}}$ (see Equation 5) to calculate the required time step Δt for the first experimental step planed with $\nu_{\text{elastic}}.$ This will reduce region II (see Figure 22) and a more accurate stress response should be expected for pure plastic region III. But beware: by a predefinition of $\Delta C_{elastic}$ the resulting total strain of the specimen has to be large enough to include the elastic range and the transition zone of elastic-plastic material behavior. Otherwise, the first section of the second experimental step planned with $v_{\text{plastic}} = 0.5$ will lead to higher strain-rates than intended. Consequently, the associated stress will be too high and approximation by means of the Ramberg-Osgood-relationship will lead to wrong results.

The flat specimen with a simple 'dog-bone'-shape (see Figure 13) was proved to be appropriate for performing stress-strain experiments. Furthermore, cooling times of $t_{8.5}$ = 6 s

were reached by natural cooling, which enables the production of a pure martensitic solid phase. It can be stated that the geometry chosen offers a workable alternative to more complex specimen geometries, as for example those suggested in [20, 21]. It should also be highlighted that the same 'dog-bone'-geometry was used to characterize the transformation induced plasticity of the same batch of S960QL steel [22] as was the case in this investigation. In both studies the same Gleeble®-3500 test system was used. This means in effect that one single specimen geometry can be used to characterize two distinct thermomechanical phenomena, which is important to minimize financial efforts and to maintain consistency in methods of experimental design and evaluation.

According to the investigations performed in [7, 12, 16], a significant influence of strain-rate on the stress-strain behavior of the S960QL steel and of the related solid phases could be observed only at temperatures upwards from 400 °C (see Figures 23-34.). By use of a constant and a temperature dependent strain-rate in this present study, the relation of the two tested strain-rates at T = 400 °C is 1:11, whereas the relation at T = 300 °C is 1:8.6 (see Table 3). Analyzing Figures 35, 36 leads to the assumption that the base material and the solid phase martensite are more susceptible to strain rates than the bainitic and austenitic phase. Unfortunately, measurement uncertainties while testing the bainitic solid phase at T = 700 °C led to missing results, so that the quantitative in-





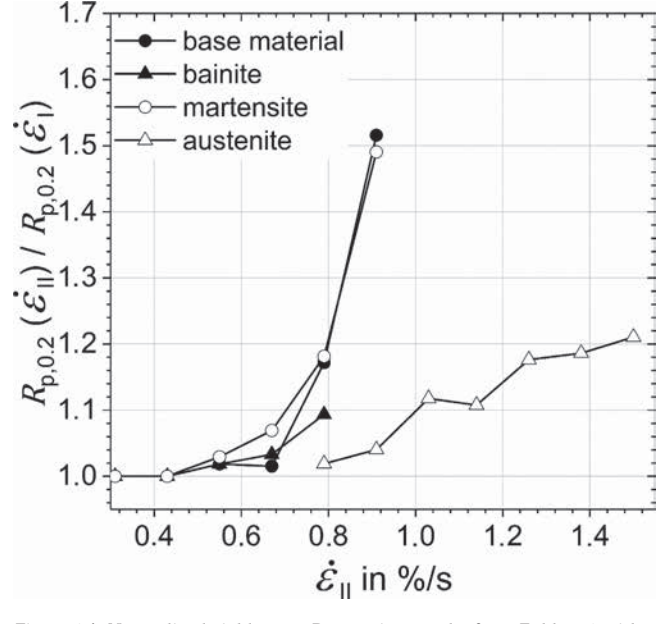


Figure 36: Normalized yield stress $R_{p,0.2}$ using results from Table 5-8 with strain-rate $\dot{\mathbf{e}}_{ll}$ according to Table 3

fluence of strain-rate at T = 700 °C on bainite cannot be analyzed. Nevertheless, for strain-rates $\dot{\epsilon}_{II}$ from 1.14 %/s up to 1.5 %/s, this means at a temperature range from 900 °C up to 1200 °C (see Table 3), the impact of increasing strain-rate $\dot{\epsilon}_{II}$ on austenitic yield stress e seems to diminish, whereas for $R_{p0.2}$ at least, a slight increase along with a growing strain-rate is visible. For this, viscous effects could be responsible.

To summarize, for users of FEA, performing numerical weld simulation under consideration of HSLA steel S9600L, two strain-rate based datasets for stress-strain behavior are provided by this study. Furthermore, if numerical welding simulation is intended, where the use of strain-rate models is neglected, the second dataset based on $\dot{\epsilon}_{\rm II}$ could be used. The meaningfulness of this recommendation should be proven by further numerical investigations.

Conclusion

In this study, the temperature dependent stress-strain behavior of transformable HSLA steel S960OL and related solid phases was successfully determined by performing strain-rate controlled experiments using a Gleeble®3500-test system. The base material as well as the solid phases bainite, martensite and austenite were tested using cost-saving flat specimen geometry.

In order to provide a material data base for numerical weld simulation, the production of the solid phases were carried out by heat treatment which is characterized by typical features of an average GMA-weld thermal cycle. To this purpose, an experimentally validated thermal numerical model of a GMA-weld joint was developed, where an average weld temperature cycle within the heat affected zone was extracted.

Two experimental series with different strain-rates were carried out. As first, a constant strain-rate at 0.05 %/s was used over the whole tested temperature range. Within the second series, experiments at a temperature dependent strain-rate from 0.1 %/s up to 1.5 %/s were conducted. Significant strain-rate dependency can only be observed beginning at temperatures of 400 $^{\circ}$ C.

With respect to non-uniform temperature distribution along the axial direction of the tested specimens, the longitudinal strain-rate was controlled by specification of the transversal strain-rate using Poisson's-ratio. Here, an adapted evaluation method for the resulting stress-strain behavior was developed where the resulting stress-strain curves

had to be approximated. Subsequently, the resulting stress-strain curves were approximated by use of the Ramberg-Osgood-relationship. By means of this experimental procedure and type of evaluation, the temperature and strain-rate dependent stress-strain behavior of metals can be characterized successfully using a Gleeble®-system.

Acknowledgements

The authors gratefully acknowledge the financial support for this research from the German Research Foundation "Deutsche Forschungsgemeinschaft – DFG". The title of the project funded was "Simulation-based effect analysis of solid state transformation on weld residual stress by use of martensitic filler materials" (Ref.-No.: SCHW 1505/4-1).

Also special thanks to the Institute of Materials and Joining Technology (IWF) at the Otto von Guericke University Magdeburg for providing the Gleeble®-3500 system.

References

- 1 L. Lindgren: Finite element modeling and simulation of welding. Part 2: Improved material modeling. J THERM STRESSES 24 (3) (2001), pp. 195-231
- DOI:10.1080/014957301300006380
- 2 U. Diekmann: Calculation of steel data using JMatPro. COMAT 21 (22) (2012):11
- 3 G. Schulze: Die Metallurgie des Schweißens: Eisenwerkstoffe-Nichteisenmetallische Werkstoffe. VDI-Buch. Springer-Verlag Berlin Heidelberg (2010) DOI:10.1007/978-3-642-03183-0
- 4 K. Easterling: Introduction to the Physical Metallurgy of Welding (Second Edition). Butterworth-Heinemann (Elsevier), Oxford (1992).
- 5 Y. Lin, X.-M. Chen: A critical review of experimental results and constitutive descriptions for metals and alloys in hot working. Materials & Design 32 (4) (2011), pp.1733-1759 DOI:10.1016/j.matdes.2010.11.048
- 6 D. Radaj: Wärmewirkungen des Schweißens: Temperaturfeld, Eigenspannungen, Verzug. Springer-Verlag Berlin Heidelberg, (1988) DOI:10.1007/978-3-642-52297-0
- 7 O. Voss: Untersuchung relevanter Einflußgrößen auf die numerische Schweißsimulation. Dissertation, Technische Universität Braunschweig, (2001)
- 8 D. Bru, J. Devaux, J. Bergheau. D. Pont: Influence of material properties at high temperatures on the modeling of welding residual stress and deformation state. In: Mathematical Modelling of Weld Phenomena 3. Verlag der Technischen Universität Graz, (1997), pp. 456-463
- 9 C. Schwenk: FE-Simulation des Schweißverzugs laserstrahlgeschweißter dünner Bleche: Sensitivitätsanalyse durch Variation der Werkstoffkennwerte. Dissertation, Technische Universität Berlin, Berlin (2007)

- 10 S. Neubert, A. Pittner, M. Rethmeier: Numerical sensitivity analysis of TRIP-parameter K on weld residual stresses for steel S355J2+N. J THERM STRESSES 39 (2) (2016), pp. 201-219 DOI:10.1080/01495739.2015.1124641
- 11 S. Neubert, A. Pittner, M. Rethmeier: Numerical Sensitivity Analysis of TRIP-Parameter-K on Weld Residual Stresses and Weld Distortion. In: Mathematical Modelling of Weld Phenomena 11. Verlag der Technischen Universität Graz, 2011), pp. 361-385
- 12 R. Ossenbrink: Thermomechanische Schweißsimulation unter Berücksichtigung von Gefügeumwandlungen. Dissertation, Brandenburgische Technische Universität Cottbus, Aachen, (2009)
- 13 H. Gnirss: Beitrag zur Ermittlung der Schweißeignung höherfester, niedriglegierter Feinkornbaustähle: Simulation von Temperaturzyklen. Dissertation, Technische Universtität Braunschweig, (1973)
- 14 V Karthik, K. Laha, K. Kasiviswanathan, B. Raj: Determination of Gradients in Mechanical Properties of 2.25 Cr-1Mo Weldments Using Shear-Punch Tests. Welding Journal (Suppl.) (2002), pp. 265-272
- 15 R. Kopp, M. De Souza, C.-M.Rogall C-M: Influence of Flow Stress Accuracy on the Results of Metal Forming Processes. Steel Res 59 (1) (1988), pp. 25-30
- 16 U. Peil, M. Wichers: Schweißen unter Betriebsbeanspruchung-Werkstoffkennwerte für einen S 355 J2G3 unter Temperaturen bis 1200° C. Stahlbau 73 (6) (2004), pp. 400-415 DOI:10.1002/stab.200490111
- 17 J. M. Bergheau, Y. Vincent, J. B. Leblond, J. F.Jullien: Viscoplastic behavior of steels during welding. Science and technology of welding and joining 9 (4) (2004), pp. 323-330 DOI:10.1179/136217104225021689
- 18 E. F. Nippes, W. F. Savage: Development of Specimen Simulating Weld Heat-Affected Zones. Welding Journal 28 (11) (1949), pp. 534-545
- 19 E. F. Nippes, W. F. Savage, B. J. Bastian, H. F. Mason, R. M. Curran: An Investigation of the Hot Ductility of High Temperature Alloys. Welding Journal 34 (4) (1955), pp.183-196
- 20 M. Abspoel, B. M. P. van Liempt: Exploring process and material parameters for hot forming. Paper presented at the 7th Forming Technology Forum, Enschede, 15 September (2014)
- 21 M. Ganapathy, N. Li, J. Lin, M. Abspoel, H. Guido, D. Bhattacharjee: Analysis of new Gleeble tensile specimen design for hot stamping application. In: MATEC Web of Conferences (2015), EDP Sciences DOI:10.1051/matecconf/20152105013
- 22 S. Neubert, A. Pittner, M. Rethmeier: Experimental determination of TRIP-parameter K for mild-and high-strength low-alloy steels and a super martensitic filler material. Springer-Plus 5 (1) (2016), pp. 1-16 DOI:10.1186/s40064-016-2474-0
- 23 J. B. Leblond, J. Devaux: A new kinetic model for anisothermal metallurgical transformations in steels including effect of austenite grain size. Acta Metallurgica 32 (1) (1984), pp. 137-146 DOI:10.1016/0001-6160(84)90211-6
- 24 D. P. Koistinen, R. E. Marburger: A general equation prescribing the extent of the austenite-martensite transformation in pure iron-

- carbon alloys and plain carbon steels. Acta Metallurgica 7 (1) (1959), pp. 59-60 DOI:10.1016/0001-6160(59)90170-1
- 25 V. A. Karkhin, P. N. Homich, V. G. Michailov: Models for volume heat sources and functional-analytical technique for calculating the temperature fields in butt welding. Mathematical Modelling of Weld Phenomena 8. Verlag der Technischen Universität Graz (2007)
- 26 J. Goldak, A. Chakravarti, M. Bibby: A New Finite Element Modell for Welding Heat Sources. Metallurgical Transactions B-Process Metallurgy 15 (2) (1984), pp. 299-305 DOI:10.1007/bf02667333
- 27 U. Peil, M. Wichers: Schweißen unter Betriebsbeanspruchung – Numerische und experimentelle Bestimmung des Temperaturfeldes beim Schweißen. Stahlbau 74 (11) (2005), pp. 843-851 DOI:10.1002/stab.200590199
- 28 S.E. Chidiac, J. K. Brimacombe, I. V. Samarasekera: A new transient method for analysis of solidification in the continuous casting of metals. Appl Sci Res 51 (3) (1993), pp. 573-597 DOI:10.1007/BF00868001
- 29 P. Seyffarth, A. Scharff: Möglichkeiten zur Vorauskalkulation von Gütewerten und Prozessdaten. Der Praktiker 50 (10) (1998), pp. 388-393
- 30 W. Ramberg, W. R. Osgood: Description of stress-strain curves by three parameters. National Advisory Committee For Aeronautics (Technical Note) 902 (1943)

Bibliography

DOI 10.3139/120.111208 Materials Testing 60 (2018) 7-8, pages 733-748 © Carl Hanser Verlag GmbH & Co. KG ISSN 0025-5300

The authors of this contribution

Dipl.-Ing. Sebastian Neubert, born 1979, studied Physical Engineering at the Technical University of Berlin, Germany, focusing on thermodynamics, fluid mechanics and numerical mathematics. After attaining his degree in 2012, he was hired as research fellow at the Bundesanstalt für Materialforschung und -prüfung (BAM) in the Division "Welding Technology". During this time at BAM, he worked in the field of numerical welding simulation. In this context, he developed material models based on extensive thermomechanical testing in order to predict the evolution of thermal stress and the formation of residual stress during GMA welding of HSLA steels.

Dr.-Ing. Andreas Pittner, born in 1980 completed his course of study in mechanical engineering at the University of Applied Sciences in Stralsund, Germany. Upon completion, he started a two years postgraduate study on computer aided mechanical engineering in Bielefeld, Germany where he specialized in software develop-

Abstract

Dehnratenabhängige Gleeble-Experimente zur Bestimmung des Spannungs-Dehnungsverhaltens des hochfesten niedriglegierten Stahls S960QL. Für die Generierung einer Materialdatenbank zur Schweißstruktursimulation wurden temperatur- und dehnratenabhängige Spannungs-Dehnungsexperimente unter Einsatz einer Gleeble®3500-Anlage durchgeführt. Als Untersuchungsgegenstand diente der hochfeste niedriglegierte Feinkornbaustahl S960QL und seine zugehörigen Festphasen Bainit, Martensit und Austenit. Zur Herstellung dieser Festphasen wurde der Grundwerkstoff Wärmebehandlungen ausgesetzt, welche die charakteristischen Merkmale eines durchschnittlichen Schweißzeittemperaturzyklus aufweisen. Dieser Temperaturzyklus wurde aus der Wärmeeinflusszone eines numerisch nachgebildeten Temperaturfeldes einer MAG-Schweißverbindung extrahiert. Die Zugversuche wurden an einer kostengünstig herzustellenden Flachprobengeometrie durchgeführt, wobei zwei Experimentalreihen mit jeweils unterschiedlichen Dehnraten realisiert wurden. Die resultierenden Spannungs-Dehnungskurven wurden durch die Ramberg-Osgood-Beziehung approximiert. Es konnte gezeigt werden, dass das temperatur- und dehnratenabhängige Spannungs-Dehnungsverhalten von Metallen durch die Anwendung eines Gleeble®-Systems erfolgreich charakterisiert werden kann. Die Einstellung der Längsdehnrate muss dabei durch die Kontrolle der Querdehnrate unter Berücksichtigung des Poisson-Verhältnisses erfolgen. Die experimentellen Prozeduren und die zugehörigen Auswertemethodiken wurden detailliert erläutert. Für alle getesteten Festphasen wurde ein signifikanter Dehnrateneinfluss erst für Temperaturen ab 400 °C aufwärts beobachtet. Die anhand der Messergebnisse abgeleiteten Ramberg-Osgood-Parameter zur Beschreibung des Verfestigungsverhaltens für den Temperaturbereich zwischen 25 °C und 1200 °C werden vollständig präsentiert.

ment and numerical mathematics. Having received his Master of Science in 2007, his started as a research fellow at the Bundesanstalt für Materialforschung und -prüfung (BAM) in Berlin. There, he focused on numerical welding simulation and the combination of phenomenological and empirical modeling approaches. In 2011 he received his doctoral degree from the Technical University of Berlin with "summa cum laude". Since 2011, he has been head of the research group "arc welding" at Division "Welding technology" at BAM. During the last years, his group has been active in the field of multivariate data analyses and arc welding control as well as structural welding simulation of large structures.

Univ.-Prof. Dr.-Ing. Michael Rethmeier studied Mechanical Engineering at the Technical Braun-

schweig University, Germany from 1993 to 1999. After working as a scientific employee and obtaining his doctoral degree at the Institute of Joining and Welding in Braunschweig in 2003, he worked as Deputy Manager of the "Fabrication Technology and Production Concepts" Division in the Corporate Research Department of Volkswagen AG in Wolfsburg, Germany. Since 2007, he has been a professor in the "Safety of Joined Components" Faculty at the Berlin University of Technology and the leader of the division "Welding Technology" at the Federal Institute for Materials Research and Testing (BAM), Berlin. Since 2009, he has also been Manager of the Joining and Coating Technology Division at the Fraunhofer Institute for Production Systems and Design Technology IPK in Berlin.